NASA TECHNICAL NOTE

NASA TN D-8418 c.l

NASA TN D-8418
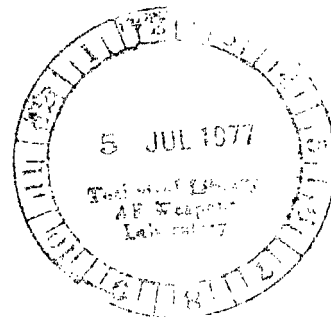
INVESTIGATION OF REAL-GAS AND VISCOUS EFFECTS ON THE AERODYNAMIC CHARACTERISTICS OF A 40° HALF-CONE WITH SUGGESTED CORRELATIONS FOR THE SHUTTLE ORBITER

James L. Hunt, Robert A. Jones, and William C. Woods

Langley Research Center
Hampton, Va. 23665

NATIONAL AERONAUTICS AND SPACE ADMINISTRATION • WASHINGTON, D. C. • JUNE 1977

1. Report No. NASA TN D-8418	2. Government Accession No.	3. Recipient's Catalog No.
4. Title and Subtitle INVESTIGATION OF REAL-GAS AND VISCOUS EFFECTS ON THE AERODYNAMIC CHARACTERISTICS OF A 40° HALF-CONE WITH SUGGESTED CORRELATIONS FOR THE SHUTTLE ORBITER		5. Report Date June 1977
		6. Performing Organization Code
7. Author(s) James L. Hunt, Robert A. Jones, and William C. Woods		8. Performing Organization Report No. L-10807
		10. Work Unit No. 505-11-31-02
9. Performing Organization Name and Address NASA Langley Research Center Hampton, VA 23665		11. Contract or Grant No.
		13. Type of Report and Period Covered Technical Note
12. Sponsoring Agency Name and Address National Aeronautics and Space Administration Washington, DC 20546		14. Sponsoring Agency Code

15. Supplementary Notes

16. Abstract

   The purpose of this paper is to evaluate parameters that might be used to correlate shuttle orbiter aerodynamic data to be used in extrapolating from wind-tunnel to flight conditions. Preliminary calculations indicate that the lee-side forces will have an insignificant influence on the aerodynamic characteristics of the orbiter for moderate angle-of-attack entries; therefore, this work is focused on phenomena which have an overriding influence on windward forces, namely, real-gas (equilibrium and nonequilibrium) and viscous-interaction effects. Analytically determined flow fields previously obtained on 40° blunted cones were used as a data source to evaluate various correlation parameters. Inviscid effects were found to be the dominant contributor to the aerodynamic coefficients (40° half-cone) in the altitude range of 64 to 76.2 km. The most suitable correlation of the aerodynamic forces on these cones is based on local dynamic pressure and local Mach number.

17. Key Words (Suggested by Author(s)) Real gas Viscous interaction Space shuttle Cone	18. Distribution Statement Unclassified – Unlimited Subject Category 02		
19. Security Classif. (of this report) Unclassified	20. Security Classif. (of this page) Unclassified	21. No. of Pages 47	22. Price* $4.00

INVESTIGATION OF REAL-GAS AND VISCOUS EFFECTS ON THE

AERODYNAMIC CHARACTERISTICS OF A 40° HALF-CONE

WITH SUGGESTED CORRELATIONS FOR THE

SHUTTLE ORBITER

James L. Hunt, Robert A. Jones,
and William C. Woods
Langley Research Center

SUMMARY

The purpose of this paper is to evaluate parameters that might be used to correlate shuttle orbiter aerodynamic data to be used in extrapolating from wind-tunnel to flight conditions. Preliminary calculations indicate that the lee-side forces will have an insignificant influence on the aerodynamic characteristics of the orbiter for moderate angle-of-attack entries; therefore, this work is focused on phenomena which have an overriding influence on windward forces, namely, real-gas (equilibrium and nonequilibrium) and viscous-interaction effects. Analytically determined flow fields previously obtained on 40° blunted cones were used as a data source to evaluate various correlation parameters. Inviscid effects were found to be the dominant contributor to the aerodynamic coefficients (40° half-cone) in the altitude range of 64 to 76.2 km. The most suitable correlation of the aerodynamic forces on these cones is based on local dynamic pressure and local Mach number.

INTRODUCTION

As a blunt body at moderate to high angles of attack enters a planetary atmosphere at hypersonic speeds, the gas molecules processed by the shock are excited to higher vibrational, chemical, and ionization energy modes, and absorb energy from the post-shock flow field. As additional energy is absorbed, the conservation laws and the thermophysics of the gas dictate certain changes in the shock-layer flow (ref. 1). The static temperature, speed of sound, and velocity in the real-gas shock layer are reduced; the density is increased and the shock-layer thickness is reduced in proportion to this increase provided dissociation is not driven near completion. The energy transfer from the shock-layer flow to the molecular energy modes and vice-versa downstream of the shock occurs at finite rates, which can be characterized by relaxation times, or by relaxation lengths in a flow of given velocity. If all relevant relaxation lengths are very much shorter than the smallest flow-field dimension of interest, the flow is regarded as being in thermochemical equilibrium (ref. 2) and the greatest departure (largest real-gas effects) from the "ideal" (nonreacting, constant ratio of specific heat γ) post-shock flow field occurs when energy is being transferred to the molecular modes. If all relevant relaxation lengths are much greater than the largest flow-field dimension of interest, the flow may be regarded as being frozen (ref. 2) so that no energy transfer

between molecular modes and the post-shock flow field occurs. In this situation the flow media may be treated as an ideal gas with constant specific heats. If relaxation lengths and flow-field dimensions are comparable, departure from thermochemical equilibrium will occur (ref. 2). The resulting nonequilibrium (finite-rate) real-gas effects on aerodynamic properties should lie between equilibrium and frozen flow provided ionization is not present.

Hypersonic wind-tunnel aerodynamics data (ideal gas) (pitching-moment coefficient C_m, drag coefficient C_D, and lift-drag ratio L/D) on slender bodies at small angles of attack have been correlated with some success on the basis of a hypersonic flat-plate viscous-interaction correlating parameter $\bar{V}'_\infty$

$$\bar{V}'_\infty = \frac{M_\infty \sqrt{C'_\infty}}{R_{\infty,l}} \qquad (1)$$

where the Chapman-Rubesin free-stream constant is

$$C'_\infty = \frac{\mu' T_\infty}{\mu_\infty T'}$$

and

M_∞ free-stream Mach number

$R_{\infty,l}$ free-stream Reynolds number based on local conditions

μ' viscosity evaluated at reference temperature

μ_∞ free-stream viscosity

T' reference temperature

T_∞ free-stream temperature

The correlation of C_m, C_D, and L/D in terms of $\bar{V}'_\infty$ for orbiter wind-tunnel data has been explained on the basis of a change in skin-friction drag. (See ref. 3.) The questions are what effect will the real-gas conditions of flight have on C_m, C_D, and L/D and to what extent will these effects influence the correlation of the aerodynamic data. Along with attempting to extend this correlation to include real-gas effects, several other factors should be considered. First, since viscous drag is sensitive to local flow conditions at the edge of the boundary layer and since these local flow conditions are changed in flight because of real-gas effects, local flow conditions should be used. Second, the effect of other factors such as lee-side pressure and real-gas effects on the windward-side pressure coefficient and thus on C_m, C_D, and L/D should be considered.

The guidelines for the task of devising credible correlating parameters are based on (1) the relative contribution to the vehicle arerodynamics of the influencing phenomena (whether inviscid, viscous, or interaction) for a given portion of the entry trajectory and (2) the fact that real-gas effects result in large changes in local boundary-layer edge conditions; therefore, any attempt to correlate aerodynamic data should begin by using local conditions to evaluate correlating parameters.

Viscous interaction parameters are derived by using local conditions at the edge of the boundary layer (ref. 4) which account for changes in the edge conditions from that of the free stream due to the vehicle angle of attack (shock processing of the flow) and accompanying inviscid real-gas effects. However, evaluating the viscous interaction parameters at the edge of the boundary layer, regardless of which weighted reference temperature is used in evaluating the Chapman-Rubesin constant C', does not account for viscous real-gas effects (dissociation and recombination in the boundary layer) which may greatly alter boundary-layer profiles and thus vehicle skin friction and induced pressure.

One way to include viscous interaction in the evaluation of orbiter real-gas effects on boundary-layer edge condition, as well as those that occur within the boundary layer due to dissociation, is to employ a partially coupled inviscid-viscous real-gas solution (equilibrium and finite rate) to calculate viscous and inviscid components of drag and pitch and correlate the results. Since these calculations for the shuttle geometry are a formidable task, the approach here was to use a simplified shape (representative of the orbiter configuration at angle of attack) for which exact solutions can be obtained. This has been done on a blunt 40° half-cone for altitudes from 64.0 to 76.2 km and is reported herein.

SYMBOLS

A	surface area
A_{pf}	element planform areas (fig. 1)
A_{tpf}	total planform area (fig. 1)
C'	Chapman-Rubesin constant based on reference temperature, $\mu(T')T/\mu(T)T'$
C^*	Chapman-Rubesin constant based on reference enthalpy, $\mu(T')h/\mu(T)h'$
$C_{D,f}$	drag coefficient due to skin friction (viscous drag)
$C_{D,p}$	drag coefficient due to pressure
$C_{D,t}$	total drag coefficient

C_m pitching-moment coefficient

$C_{m,f}$ moment coefficient due to skin friction

$C_{m,fD}$ moment coefficient due to skin-friction drag

$C_{m,p}$ moment coefficient due to pressure

$C_{m,pD}$ moment coefficient due to pressure drag

$C_{m,t}$ total pitching-moment coefficient

C_p pressure coefficient

D drag

h enthalpy

h^* reference enthalpy, $0.5h_w + 0.22h_{aw} + 0.28h$

L lift

l length from nose apex to local position

l_c cone axial length (fig. 13)

l_{ref} reference cone length (table III)

l_{rpf} reference planform length (fig. 1)

l_v vehicle length

M Mach number

m_i element moment arm to center of gravity (fig. 1)

p static pressure

$p_{t,2}$ total pressure behind normal shock

q dynamic pressure

R Reynolds number

r_b cone base radius

r_n cone nose radius

S_{pf} reference planform area (fig. 1)

S_{ref} one-half cone base area

T static temperature

T' reference temperature, $\quad T\left[1 + 0.0225\ \dfrac{\gamma - 1}{2}\ M^2 + \left(0.695\ \dfrac{T_w}{T_\infty} - 1\right)\right]$

u velocity

$\overline{V}'$ viscous interaction parameter, $\quad M\sqrt{C'}\big/\sqrt{R}$

x axial distance

y distance normal to cone surface

Z positive normal-force direction

α angle of attack

γ ratio of specific heats

γ_{ie} isentropic exponent, $\quad \dfrac{d \log p}{d \log \rho}$

δ flow deflection angle

θ cone half-angle

μ viscosity

ρ density

ϕ cone-ray meridian angle

Subscripts:

aw   adiabatic wall

Eq   equilibrium

e   boundary-layer edge

FR   finite rate

l based on local conditions (at $x/l_c = 0.5$ for cone analysis (fig. 13))

l_c based on cone length

q_l coefficient (drag or pitch) nondimensionalized by local dynamic pressure at $x/l_c = 0.5$

t   total

w   wall

2   based on local conditions behind oblique shock

∞   based on free-stream conditions

Abbreviations:

CFHT   continuous flow hypersonic tunnel

Eq   equilibrium

FR   finite rate

VDT   variable density tunnel

Primes denote quantity evaluated at reference temperature.

ROUGH ESTIMATES OF EFFECTS OF FLIGHT CONDITIONS

Leeward Pressure Effects

To obtain a rough order of magnitude estimate of the effect of lee-side pressure on orbiter pitching moment, an estimate was made by assuming constant pressures to act over the plan view with the geometry of figure 1. With zero pressure coefficient for the lee side at an angle of attack of 40° and $C_p = 1.05$ on the windward side ($\gamma = 1.4$ ideal-gas oblique shock value for $M_\infty = 20$), the pitching-moment coefficient C_m is -0.54. Changing the lee side C_p to ±0.03 rather than zero gives only a 3-percent change in C_m. Therefore, it is felt that any M_∞, R_∞, and real-gas effects would have only a small effect on the lee-side contribution to C_m.

Furthermore, one estimate of real-gas effects on lee-side pressure indicates that ideal gas air data may be applicable to flight provided the correct Mach number and Reynolds number are simulated. This estimate was on the basis of finite-rate chemistry calculations made under contract for shuttle conditions (ref. 5). They were given an assumed pressure distance variation for expansion from the windward to the leeward side (fig. 2) and a flight condition of 6.1 km/sec at an altitude of 67.1 km, and $\alpha = 20°$. The calculated results for both equilibrium and nonequilibrium (finite-rate) real air are shown in figure 3. On the windward side, at the start of the expansion the isentropic

exponent is 1.12. If the real gas were to expand around the vehicle and remain in equilibrium, the isentropic gamma (d log p/d log ρ) remains constant at 1.12 as indicated by the slope of the curve in figure 3; however, the finite-rate chemistry calculations showed that for the data of figure 2, the gas would actually "freeze" and follow the nonequilibrium (finite-rate) line shown in figure 3 which has a slope, and thus a gamma, of 1.43. This result indicates that to best match the pressure/density relation in an expansion to the lee side in flight at this one condition, one should test in an ideal gas having a gamma of 1.43 at the correct Mach number and Reynolds number. In other words, conventional air wind tunnels may give the best simulation for this one flight condition.

Real-Gas Effect on Windward Pressure Coefficient

A rough estimate of the effects on C_m due to changes in C_p on the windward side of the orbiter was made by using the constant-pressure planform approach shown in figure 1. The magnitude of real-gas effects on C_p for oblique shocks is shown in figure 4. Here C_p is shown for several ideal gas values of gamma at Mach 20 (oblique shock calculations for gamma of 1.1, 1.4, and 1.67) and for an equilibrium real gas (realistic for orbiter windward wide) at an altitude of 60 964 m and a velocity of 6096 m/sec (ref. 6). For small deflection angles real-gas effects are small, but they become large as the flow deflection angle increases. For an oblique shock at $\delta = 40°$ which corresponds to $\alpha = 40°$, the real-gas C_p is 0.95 whereas the ideal-gas air value at $M_\infty = 20$ is 1.05. Integrating as shown in figure 1 indicates that the ideal gas C_m is -0.054 whereas the equilibrium real-gas C_m is -0.049, a 10-percent change.

A better estimate of the real-gas effect could be made by using wind-tunnel test data at various effective gammas. The effective value of gamma (isentropic exponent (ref. 6)) in the shock layer for flight varies over the trajectory as shown in figure 5. This value varies from about 1.1 to 1.24 during the high-velocity high α part of entry. The Langley hypersonic CF_4 tunnel (ref. 7) is capable of obtaining force and moment data on a model of the orbiter at these effective gammas.

Questions arise as to how gamma varies over the windward side in the shock layer and over the trajectory. Figure 6 may help to show the relative insensitivity of gamma for the orbiter flight conditions. This figure is taken from reference 8. The value of γ remains approximately constant for a wide range of velocities and is only weakly affected by pressure for orbiter hypersonic entry conditions (matches CF_4 tunnel).

Real-Gas Effect on Elevon Effectiveness

The downward deflection of the elevon of the orbiter during hypersonic flight will generate an embedded shock. The inviscid real-gas effects on C_p ratio for this condition are shown in figures 7 (flight fairing from ref. 9)

and 8 and compared with that for ideal-gas wind tunnels. As shown, the presence of the embedded shock causes large differences in the elevon pressure ratio between real-gas and wind-tunnel conditions.

Another factor which complicates this analysis is the possibility of separation of the low Reynolds number boundary-layer flow due to the adverse pressure gradient. Extensive boundary-layer separation could result in greatly reduced elevon effectiveness.

CORRELATION OF ORBITER HYPERSONIC AERODYNAMIC DATA

Similitude Parameters

Real-gas effects result in large changes in local Mach number behind oblique shock M_2, local Reynolds number R_2, as well as in C'. The resulting changes in the correlating parameters

$$
\left.\begin{aligned}
\overline{V}'_\infty &= \frac{M_\infty \sqrt{C'_\infty}}{\sqrt{R_{\infty,\, l_V}}} \\[2ex]
\overline{V}_2 &= \frac{M_2 \sqrt{C'_2}}{\sqrt{R_2}}
\end{aligned}\right\}
\tag{2}
$$

are shown in figures 9 to 12 and compared with the values for an orbiter trajectory as well as the values that can be obtained in several wind-tunnel facilities. Obviously, for either $\overline{V}_\infty$ or $\overline{V}_2$, if Mach number and Reynolds numbers are matched, $\overline{V}'$ is simulated rather closely. However, just matching $\overline{V}'$ does not mean that Mach number and/or Reynolds number are matched. As can be seen by comparing figures 9 and 10, it is possible to test at flight $\overline{V}'_\infty$ or $\overline{V}'_2$ and be in error in both Mach number and Reynolds number. Since aerodynamic similitude in ideal gas requires the duplication of M_e, R_e, and T_w/T_t, the question becomes that of the degree of coupling between these so-called independent parameters. Also, the question as to which forces are dominant (inviscid, viscous, or interaction) must be addressed before a correlation parameter can be selected for the total (inviscid or viscous) aerodynamic characteristics of a vehicle.

The viscous interaction parameter $\overline{V}'_\infty$ may be a good parameter for correlating ideal-gas hypersonic aerodynamic data for a given γ test media; however, it is probably a poor correlation parameter for flight-entry hypersonic aerodynamic data for the following reasons: (1) Viscous effects are dependent on the boundary-layer profiles which are, in turn, influenced by the chemical reaction in the boundary layer. A viscous interaction parameter cannot account for these influences. (2) Viscous effects are governed by the local conditions at the edge of the boundary layer (not free stream) and real-gas effects greatly alter these local conditions in flight as compared with those in ground facilities (figs. 11 and 12). A viscous interaction parameter based on free-stream conditions cannot account for these alterations. (3) The real-gas influence

on pressure level and distribution probably has a larger effect on the aero-
dynamic coefficients than viscous interaction over a significant part of the
entry trajectory.

Flow-Field Solution Technique

Since aerodynamic center of pressure shifts due to real-gas effects and
viscous interactions along with changes in control surface effectiveness may
alter the trim condition of the vehicle, it is imperative that the shuttle
orbiter aerodynamic correlation parameters be properly evaluated. One means
of evaluating these real-gas and viscous interaction effects is to employ a
partially coupled inviscid-viscous real-gas solution to calculate viscous and
inviscid components of drag and pitch on the orbiter, but this is a formidable
task; therefore, one approach is to make such calculations on a simplified con-
figuration at orbiter flight conditions and correlate the results. Such cal-
culations have been made on a blunt 40° cone. The flow-field calculations are
axisymmetric but the aerodynamic coefficients were obtained by integrating over
one-half the cone. Viscous and inviscid components of drag and pitch were
obtained by using quasi-coupled inviscid-viscous real-gas solutions of a
40° half-angle cone (fig. 13) for both orbiter flight conditions (altitudes
of 64.0 and 76.2 km) and representative tunnel tests.

The flow-field solutions (equilibrium and finite-rate) required in obtain-
ing the flow-field results presented in tables I to IV were calculated by using
previously developed computer codes to define inviscid and viscous flow fields.
The computer codes utilized (NASA Ames equilibrium blunt body and method of
characteristics, modified Curtis and Strom unified nonequilibrium flow field,
and a modified version of the viscous reacting gas code developed by Blottner)
and the manner in which they were applied are given in reference 10. The pro-
cedure utilized in reference 10 was not fully coupled in that the inviscid phase
(inviscid flow-field properties) and viscous phase (boundary layer) were com-
puted separately; however, these two independent phases were interfaced through
a viscous-inviscid mass flux matching in the shock layer along points at the
edge of the boundary layer. Initial estimates of the edge conditions for the
boundary layer were made and the computation carried out. The resulting
boundary-layer mass flow was then used to interpolate along the previously
computed inviscid field rays to determine flow conditions in the inviscid field
at a point corresponding to the boundary-layer mass flow value. The results
herein are thus subject to the qualification that the boundary-layer displace-
ment thickness effects (displacement thickness corrections to the cone surface
contour) are small, and at least for the cases analyzed (tables I to V), the
displacement thickness correction need not be considered in the inviscid flow-
field computation.

Objective

The objective of this effort is to correlate viscous interaction and real-
gas effects for orbiter-like entry and tunnel conditions (analytical, no experi-
ment) for the purpose of extrapolating tunnel aerodynamic data to flight condi-
tions. The assumption herein is that parameters which correlate the aerodynamic

data on this simplified configuration ($40°$ half-angle cone) should also be applicable to the shuttle orbiter at entry conditions; therefore, the emphasis of this paper is on selecting an appropriate set of correlation parameters for the $40°$ half-angle cone aerodynamic coefficients. (See tables I to V.) Such correlations are critical to the successful prediction of the orbiter aerodynamic characteristics during entry since aerodynamic center shifts due to real-gas effects not yet accounted for and viscous interaction improperly correlated along with changes in control surface effectiveness may alter the trim conditions of the vehicle.

The guidelines for this task of devising correlating parameters are based on (1) the relative contribution to the vehicle aerodynamics of the influencing phenomena (whether inviscid, viscous, or interaction) for a given section of the entry trajectory and (2) the fact that real-gas effects result in large changes in local boundary-layer edge conditions. Therefore, local conditions must be considered in evaluating correlating parameters.

RESULTS AND DISCUSSION

Both inviscid and laminar viscous (coupled) real-gas (equilibrium and nonequilibrium) flows were calculated for a series of blunt cones ($\theta = 30°$ and $40°$, $\iota/r_n = 50$ and 100) at orbiter flight conditions (64.0 km $\leqq$ altitude $\leqq 76.2$ km, $4.9 \leqq$ velocity $\leqq 7.3$ km/sec) as well as for ideal-gas conditions in several wind tunnels (ref. 10). The skin friction and pressure were integrated over one-half of the surface of the $40°$ half-angle cone ($\iota_c/r_n = 50$, fig. 13) for the various cases already computed (ref. 10) along with computing several local parameters for correlative purposes. The results are given in tables I to V.

Viscous Interaction Parameters

Since hypersonic wind-tunnel aerodynamic data on slender bodies at small angles of attack have been correlated with some success on the basis of the hypersonic viscous interaction correlating parameter $\overline{V}'_\infty$, the viscous coefficients on the $40°$ half-angle cone (fig. 13) will be first examined on the basis of this parameter. Figures 14 and 15 show the viscous drag and pitching-moment coefficients as a function of $\overline{V}'_\infty$ for both the flight and tunnel calculated data on the $40°$ half-angle cone. The data correlate well on a straight line except for the Mach 20 nitrogen tunnel data. The same coefficients are shown in figures 16 and 17 as a function of $\overline{V}'$ based on local coefficients at $x/\iota_c = 0.5$. The data for both viscous drag and pitching-moment coefficients including the Mach 20 nitrogen tunnel cases correlate along a straight line and indicate that a better correlation of the viscous coefficients is obtained with a $\overline{V}'$ based on local conditions ($x/\iota_c = 0.5$) rather than on free-stream values.

If local conditions are to be used in the correlation, then the aerodynamic coefficients themselves should be formulated with a local dynamic pressure rather than with the free-stream dynamic pressure. Thus, the viscous drag coefficient based on the local dynamic pressure external to the boundary

10

layer at an $x/l_c = 0.5$ is given in figure 18 as a function of $\bar{V}'_l$. Here the flight and CF_4 tunnel data (ref. 10) correlate along one straight line whereas the remaining wind-tunnel data correlate along a different straight line. There are probably two reasons for this difference: (1) local M_e, R_e, and T_w/T_t are independent simulation parameters and they are not coupled into one independent simulation parameter by $\bar{V}'_l$ and (2) boundary-layer edge conditions are similar in flight and in the CF_4 tunnel. The second stems from the fact that viscous effects not only depend on the boundary-layer edge conditions but on boundary-layer profiles which are in turn influenced by the chemical reaction in the boundary layer. This result is supported by the boundary-layer temperature profiles shown in figure 19. The profile shown for CF_4 at $M_\infty = 6$ is much more similar to the two flight profiles shown than those calculated in air, helium, and nitrogen hypersonic tunnels.

<div align="center">Relative Contribution of Phenomena Influencing</div>

<div align="center">Aerodynamic Coefficients</div>

Before attempting a correlation of the total (inviscid plus viscous) aerodynamic coefficients, the question that must be considered is what percentage of the aerodynamic coefficient is contributed by specific influencing phenomena (whether inviscid, viscous, or interaction). The percent of the drag coefficient contributed by the viscous, finite-rate, and real-gas effects is shown in figure 20 as a function of $\bar{V}'_\infty$. For flight conditions from an altitude of 64.0 to 76.2 km, viscous effects account for only 1 to 2 percent of the total drag coefficient. Finite-rate effects are even smaller. The differences in tunnel and flight drag coefficients (fig. 20) indicate that the real-gas effects in flight account for approximately 10 percent of the total drag.

The percentage contribution to the pitching-moment coefficient is given in figure 21. The viscous effects account for 4 to 10 percent of the total pitching-moment coefficient, finite-rate effects again being smaller. Real-gas effects are on the order of 5 to 11 percent or essentially the same as the viscous effects. The obvious implication is that the influencing phenomena of the total aerodynamic coefficients for this cone angle in this flight regime are 90 to 98 percent inviscid; therefore, the proper correlation must rely heavily on inviscid parameters. At higher altitudes or smaller cone angles viscous effects could become more significant.

<div align="center">Data Spread</div>

The inviscid drag coefficients for both flight and wind-tunnel conditions are given in figure 22 as a function of $\bar{V}'_\infty$. The flight data lie in the lower left-hand corner whereas the wind-tunnel data are spread out along the top of the plot. Obviously, $\bar{V}'_\infty$ does not correlate the inviscid drag; however, the spread is only approximately 8 percent (real-gas effects). Thus, in searching for a more suitable correlation parameter which according to the previous section must rely heavily on inviscid parameters, a fine tuning is required since small percentage scatter is involved. Therefore, the criterion for a correlation parameter is that the scatter of the data is less than 10 percent.

11

Free-Stream Inviscid Correlation Parameter

A correlation of the pressure coefficient based on free-stream γ and M as suggested by the hypersonic similarity law (ref. 11) is given in figure 23. This correlation is not acceptable since the data scatter is much greater than 10 percent in the flight part of the curve. Also, the fairing is strongly nonlinear which makes extrapolation from wind tunnel to flight conditions inaccurate. This is very significant here since in an actual extrapolation of shuttle orbiter wind-tunnel data, flight data points are not available. Thus, depending on how the tunnel data are faired ($M_\infty \leqq 20$), extrapolation errors of 20 to 30 percent are possible for flight Mach numbers in the Mach 25 to 30 range. (See fig. 23. Use of Mach 20 helium data points would make tunnel-data extrapolation error much larger.)

Local Inviscid Correlation Parameter

Inviscid similitude at geometrically similar points in model and prototype compressible fluid flow systems requires duplication of Mach number and the isentropic exponent (gamma); therefore, an inviscid correlation parameter should contain both Mach number and gamma. Prior discussion of real-gas effects herein also indicates that the correlation parameter should be based on some local reference conditions behind the bow shock and not on free-stream conditions.

It was surmised in the section "Viscous Interaction Parameters" that if local conditions are to be used in the correlation, then the aerodynamic coefficients themselves should be formulated with a local dynamic pressure rather than with the free-stream value.

Examining the inviscid drag coefficient

$$(C_{D,p})_{q_l} = \frac{\int p \, dA}{\frac{1}{2}\rho_l u_l^2 A} = \frac{\int p \, dA}{\frac{\gamma_l}{2} p_l M_l^2 A} \tag{3}$$

where γ is now the isentropic exponent. For a sharp cone with no viscous effects, $(C_{D,p})_{q_l}$ becomes

$$(C_{D,p})_{q_l} = \frac{p_l \int dA}{\frac{\gamma_l}{2} p_l M_l^2 A} = \frac{2}{\gamma_l M_l^2} \tag{4}$$

Even though the pressure canceled out (eq. (4)), which it will not do for the real situation since bluntness and induced pressure keep the cone pressure p inside the integral (eq. (3)), the parameter $(C_{D,p})_{q_l}$ or $(C_{m,p})_{q_l}$ should,

when plotted against local Mach number, collapse the gamma effects. The corre-
lation is in essence

$$\frac{2 \int p \, dA}{p_l A} = \gamma_l M_l^2 f(M_l) \tag{5}$$

The pressure drag coefficient based on the local dynamic pressure at
$x/l_c = 0.5$ is given as a function of local Mach number in figure 24. This
correlation shows promise since the scatter of the data is less than 3 per-
cent about a linear fairing of tunnel and flight data points (the Mach 20
helium data point which is farthest from the flight part of the fairing being
neglected). Also, the tunnel data fairing is very near linear in the flight
part of the fairing where the CF_4 tunnel data point lies; this linearity would
probably allow a more accurate extrapolation of wind-tunnel data to flight
conditions.

The inviscid pitching moment based on local dynamic pressure is given as
a function of local Mach number in figure 25. The data spread about the lin-
ear fairing of flight and tunnel data is approximately 4 percent and the fair-
ing of tunnel data is again near linear in the flight part.

The total drag and pitching-moment coefficients based on local dynamic
pressure are given as a function of local Mach number in figures 26 and 27,
respectively. The data spread about the linear fairing in the drag coeffi-
cient correlation is less than 3 percent. The spread is slightly larger in
the pitching-moment correlation; however, the correlation is extremely good in
the flight data region. Also, finite-rate flight data correlated equally as
well as equilibrium flight data.

Space Shuttle Orbiter Correlation and Extrapolation

to Flight Condition

The correlation of total pitch and drag nondimensionalized by local dynamic
pressure as a function of local Mach number was extremely good for the case of
the 40° half-angle cone in that the data spread about data fairing was less than
or equal to 3 percent; the tunnel-data fairings were near linear and the CF_4 tun-
nel data point for both pitch and drag lay within the flight local Mach number
regime which makes the extrapolation to flight conditions amenable. Also
finite-rate flight data correlated equally as well as equilibrium flight data.
This result leads to the question of how such a correlation based on local con-
ditions is established for the shuttle.

First, aerodynamic wind-tunnel data are obtained on the orbiter configu-
ration for a given angle of attack at hypersonic Mach numbers in helium, air,
nitrogen, tetrafluoromethane (CF_4), and hexafluoromethane (C_2F_6 postulated
tunnel). Hexafluoromethane has been included because, according to figures 10
and 12, a local Mach number significantly higher than that which occurs at

13

Mach 6 in CF_4 could be obtained. This condition would result in two experimental wind-tunnel data points (CF_4 and C_2F_6) in the flight section of the pitch and drag fairing (figs. 24 to 27) and thus would lend much more credibility and accuracy in extrapolation of the correlation. In fact, for the altitude range of this study (64 km to 762 km), the addition of a data point in C_2F_6 would alleviate the need for practically any extrapolations.

Second, the local properties on a cone or wedge with a cone or wedge angle compatible with the particular orbiter angle of attack would be calculated for each tunnel condition. These calculated local properties (dynamic pressure and Mach number) at an appropriate reference station would be used in correlating the orbiter aerodynamic forces. The idea here being that the change in windward free stream to local conditions for the orbiter at some reference station downstream of the influence of the apex flow could be represented by the change in free stream to local conditions of a cone or wedge (with a half-angle equal to the orbiter angle of attack) at the same tunnel conditions. A test program to establish and validate this correlation for the orbiter in the manner described is being pursued.

Once the correlation has been established with wind-tunnel aerodynamic data on the orbiter by using the local Mach number and dynamic pressure calculated at the reference location for an appropriate cone or wedge, the local conditions on an appropriate cone or wedge at the assigned reference location are calculated along the flight trajectory (equilibrium and finite rate). These local conditions (equilibrium and finite rate) are used to enter the correlation established with wind-tunnel data to obtain the orbiter flight aerodynamics. This procedure must be repeated for each angle of attack.

Aerodynamic Coefficient Correlation for Altitudes Above

76.2 km and Angle of Attack Lower Than 40°

Real-gas effects are extremely sensitive to the angle of attack of the vehicle. Decreasing the cone angle below 40° (representing a reduction in the orbiter angle of attack) for the 64- to 76.2-km altitude range of this study will both decrease the real-gas effects and increase the viscous influence on the aerodynamic characteristics. Thus, for some lower angle of attack the correlation advocated in the previous section may break down and a $\bar{V}'$ based on local conditions may serve to correlate the aerodynamic coefficients. If the angle of attack and velocity are small enough, a correlation with a $\bar{V}'$ based on free-stream conditions may be needed.

At altitudes above 76.2 km for a shuttle orbiter type entry, both finite-rate and viscous effects will become more dominant. Here again, the local Mach number correlation may collapse but the importance of using local conditions in viscous correlation parameters will probably become more pronounced. One possible solution to the correlation problem as the viscous effects become more pronounced is to establish local inviscid correlations such as suggested herein for constant levels of viscous effects as indicated by either $\bar{V}_l'$ or R_l.

CONCLUSIONS

These conclusions apply to a 40° half-angle blunt half-cone entry along an orbiter trajectory in the altitude range from 64 to 76.2 km. Trends indicated here should be applicable to the shuttle orbiter at an angle of attack of 40°.

(1) Aerodynamic coefficient (drag and pitch) data spread (tunnel and flight) is reduced from an 8- to 10-percent spread to a 3- to 4-percent spread by using an inviscid correlation based on local conditions.

(2) Viscous effects account for 1 to 2 percent of total drag and 4 to 10 percent of total pitching moment.

(3) Finite-rate effects account for 0.1 to 2 percent of total drag coefficient and 0.1 to 5 percent of total pitching-moment coefficient.

(4) Real-gas effects are on the order of 10 percent for both drag and pitching moment.

(5) The viscous interaction parameter $\bar{V}'$ appears to be a poor correlation parameter for hypersonic entry of large angle cones. There are three causes for this condition:

  (a) Viscous effects are governed by the local conditions at the edge of the boundary layer (not free stream) and real-gas effects greatly alter these local conditions in flight as compared with those in ground facilities.

  (b) The viscous effects are dependent on the boundary-layer profiles which are, in turn, influenced by the chemical reaction in the boundary layer.

  (c) A viscous interaction parameter based on free-stream conditions cannot account for changes in pressure level and distribution which occur because of real-gas effects. This change in pressure has a larger effect on the aerodynamic coefficients than viscous interaction over a significant part of the trajectory.

Langley Research Center
National Aeronautics and Space Administration
Hampton, VA 23665
February 9, 1977

REFERENCES

1. Hunt, James L.; Jones, Robert A.; and Smith, Kathryn A.: Use of Hexafluoro-
   ethane To Simulate the Inviscid Real-Gas Effects on Blunt Entry Vehicles.
   NASA TN D-7701, 1974.

2. Bray, K. N. C.: Real Gas Effects on Lifting Reentry Aerothermodynamics.
   Aerodynamic Problems of Hypersonic Vehicles, Volume 1, R. C. Pankhurst,
   ed., AGARD-LS-42-Vol-1, July 1972.

3. Whitfield, Jack D.; and Griffith, B. J.: Viscous Effects on Zero-Lift Drag
   of Slender Blunt Cones. AEDC-TDR-63-35, U.S. Air Force, Mar. 1963.

4. Sieron, Thomas R.; and Martinez, Conrad, Jr.: Effects and Analysis of Mach
   Number and Reynolds Number on Laminar Skin Friction at Hypersonic Speeds.
   AFFDL-TR-65-5, U.S. Air Force, Apr. 1965. (Available from DDC as
   AD 465 764.)

5. Lordi, John A.; Vidal, Robert J.; and Johnson, Charles B.: Chemical Non-
   equilibrium Effects on the Inviscid Flow in the Windward Plane of Symmetry
   of Two Simplified Shuttle Configurations. NASA TN D-7189, 1973.

6. Hunt, James L.; and Souders, Sue W.: Normal- and Oblique-Shock Flow Param-
   eters in Equilibrium Air Including Attached-Shock Solutions for Surfaces
   at Angles of Attack, Sweep, and Dihedral. NASA SP-3093, 1975.

7. Jones, Robert A.; and Hunt, James L. (with appendix A by James L. Hunt,
   Kathryn A. Smith, and Robert B. Reynolds and appendix B by James L. Hunt
   and Lillian R. Boney): Use of Tetrafluoromethane To Simulate Real-Gas
   Effects on the Hypersonic Aerodynamics of Blunt Vehicles. NASA TR R-312,
   1969.

8. Jorgensen, L. H.: Charts of Isentropic Exponent as a Function of Enthalpy
   for Various Gases in Equilibrium. NASA SP-3020, 1965.

9. Nagel, A. L.; and Thomas, A. C.: Analysis of the Correlation of Wind
   Tunnel and Ground Test Data to Flight Test Results. AIAA paper
   No. 65-208, Feb. 1965.

10. Fivel, H. J.; Masek, R. V.; and Mockapetris, L. J.: Analytical Comparison
    of Hypersonic Flight and Wind Tunnel Viscous/Inviscid Flow Fields. NASA
    CR-2489, 1975.

11. Shapiro, Ascher H.: The Dynamics and Thermodynamics of Compressible Fluid
    Flow. Vol. II, Ronald Press Co., c.1954.

TABLE I.- FLIGHT CONDITIONS

Altitude, km	Velocity, km/sec	l_c/r_n	θ, deg	State	Free-stream conditions				Local conditions $\left(x/l_c = 0.50\right)$			
					M_∞	R_{∞,l_c}	C'_∞	$\bar{V}'_\infty$	M_l	R_l	C'_l	$\bar{V}'_l$
76.2	7.315	50	40	Equilibrium	26.1	0.9540×10^6	0.4773	0.01911	4.038	0.4050×10^6	1.167	0.00687
70.104	7.315	50	40	Equilibrium	24.64	2.0940	.5055	.01240	3.955	.9350	1.171	.00443
64.008	6.096	50	40	Equilibrium	19.50	3.5014	.5239	.00766	3.762	1.8584	1.162	.00298
64.008	4.877	50	40	Equilibrium	15.60	2.8102	.5683	.00713	3.630	1.8141	1.141	.00288
76.2	7.315	50	40	Nonequilibrium	26.1	.9540	.4773	.01911	3.565	.2600	1.186	.00762
70.104	7.315	50	40	Nonequilibrium	24.64	2.0940	.5055	.01240	3.174	.4919	1.177	.00492
64.008	6.096	50	40	Nonequilibrium	19.50	3.5014	.5239	.00766	3.762	1.8584	1.162	.00298
64.008	4.877	50	40	Nonequilibrium	15.60	2.8102	.5683	.00713	3.630	1.8141	1.141	.00288

Altitude, km	Velocity, km/sec	l_c/r_n	θ, deg	State	Reference conditions			Pressure data				Skin-friction data			
					q_∞, kN/m²	l_{ref}, m	S_{ref}, m²	Drag force, MN	$C_{D,p}$	Moment, MN-m	$C_{m,p}$	Drag force, kN	$C_{D,f}$	Moment, kN-m	$C_{m,f}$
76.2	7.315	50	40	Equilibrium	1.068	30.48	1050.55	0.949	0.84623	-2.991	-0.08747	18.69	0.01666	-307.64	-0.00900
70.104	7.315	50	40	Equilibrium	2.639	30.48	1050.55	2.348	.84714	-7.400	-.08758	29.33	.01058	-482.86	-.00571
64.008	6.096	50	40	Equilibrium	4.067	30.48	1050.55	3.634	.85036	-11.453	-.08793	28.13	.00658	-463.13	-.00356
64.008	4.877	50	40	Equilibrium	2.603	30.48	1050.55	2.335	.85395	-7.374	-.08847	16.23	.00593	-267.20	-.00321
76.2	7.315	50	40	Nonequilibrium	1.068	30.48	1050.55	.936	.83531	-2.859	-.08368	16.36	.01459	-269.29	-.00788
70.104	7.315	50	40	Nonequilibrium	2.639	30.48	1050.55	2.330	.84058	-7.339	-.08686	24.38	.00800	-401.34	-.00475
64.008	6.096	50	40	Nonequilibrium	4.067	30.48	1050.55	3.633	.85027	-11.458	-.08798	26.64	.00623	-437.03	-.00337
64.008	4.877	50	40	Nonequilibrium	2.603	30.48	1050.55	2.335	.85395	-7.374	-.08846	15.76	.00576	-269.29	-.00311

TABLE II.- WIND-TUNNEL CONDITIONS

Test gas	l_c/r_n	θ, deg	Free-stream conditions				Local conditions $\left(x/l_c = 0.5\right)$			
			M_∞	R_{e,∞,l_c}	C'_∞	$\bar{V}'_\infty$	M_l	R_l	C'_l	$\bar{V}'_l$
Air	50	40	8	1.2955×10^6	0.95172	0.00686	2.066	0.5656×10^6	1.0433	0.00285
Air	50	40	8	7.7728	.95172	.00230	2.066	3.3920	1.0433	.00114
Nitrogen	50	40	20	.0576	1.2424	.09237	2.208	.0102	1.1875	.02380
Nitrogen	50	40	20	.2231	1.2424	.04720	2.207	.0396	1.1875	.01208
Helium	50	40	20	1.9071	.24187	.00712	1.585	.1681	.9800	.00388
Freon	50	40	6.2	.0496	.95511	.02721	3.166	.0930	1.0339	.01056
Freon	50	40	6.2	.2978	.95611	.01111	3.166	.5580	1.0339	.00434

Test gas	l_c/r_n	θ, deg	Reference conditions			Pressure data				Skin-friction data			
			q_∞, kN/m²	l_{ref}, m²	S_{ref}, m²	Drag force, kN	$C_{D,p}$	Moment, N-m	$C_{m,p}$	Drag force, N	$C_{D,f}$	Moment, N-m	$C_{m,f}$
Air	50	40	16.591	0.2134	0.0513	0.731	0.90015	-15.519	-0.08952	4.048	0.00499	-0.461	-0.00269
Air	50	40	94.918	.2134	.0513	4.388	.90044	-96.046	-.09237	10.186	.00209	-1.166	-.00113
Nitrogen	50	40	.807	.1524	.0262	.019	.90125	-.298	-.09077	1.201	.05613	-.095	-.03031
Nitrogen	50	40	3.229	.1524	.0262	.074	.87397	1.101	-.08784	2.358	.02765	-.190	-.01493
Helium	50	40	10.991	.2134	.0513	.512	.90744	10.741	-.09090	3.292	.00579	-.380	-.00313
Freon	50	40	1.055	.2134	.0513	.049	.89808	1.058	-.09155	1.246	.02272	-.136	-.01227
Freon	50	40	6.328	.2134	.0513	.292	.89818	6.305	-.09099	3.025	.00093	-.353	-.00499

TABLE III.- DRAG FORCE MOMENT FOR FLIGHT CONDITIONS

Reference conditions				Pressure data		Skin-friction data	
q_∞, kN/m^2	l_{ref}, m	S_{ref}, m^2	State	Drag force moment, MN-m	$C_{m,pD}$	Drag force moment, kN-m	$C_{m,fD}$
1.068	30.48	1055.55	Equilibrium	-10.403	-0.30422	185.218	-0.00542
2.639	30.48	1055.55	Equilibrium	-25.733	-.30456	290.728	-.00344
4.067	30.48	1055.55	Equilibrium	-26.261	-.30573	278.867	-.00214
2.603	30.48	1055.55	Equilibrium	-25.598	-.30708	162.454	-.00195
1.068	30.48	1055.55	Nonequilibrium	-10.223	-.29920	162.197	-.00475
2.639	30.48	1055.55	Nonequilibrium	-25.533	-.30219	246.461	-.00292
4.067	30.48	1055.55	Nonequilibrium	-26.259	-.30571	265.727	-.00204
2.603	30.48	1055.55	Nonequilibrium	-25.596	-.30708	157.722	-.00189

TABLE IV.- DRAG FORCE MOMENT FOR WIND-TUNNEL CONDITIONS

Reference conditions				Pressure data		Skin-friction data	
q_∞, kN/m^2	l_{ref}, m	S_{ref}, m^2	Test gas	Drag force moment, N-m	$C_{m,pD}$	Drag force moment, N-m	$C_{m,fD}$
16.591	0.2134	0.0513	Air	-55.751	-0.32181	-0.271	-0.00160
94.918	.2134	.0513	Air	-335.999	-.32314	-.691	-.00066
.807	.2134	.0513	Nitrogen	-1.044	-.32274	-.054	-.01815
3.229	.2134	.0513	Nitrogen	-4.027	-.31289	-.108	-.00891
10.991	.2134	.0513	Helium	-39.102	-.32475	-.230	-.00185
1.055	.2134	.0513	Freon	-3.715	-.32205	-.081	-.00735
6.328	.2134	.0513	Freon	-22.317	-.32185	-.203	-.00299

TABLE V.- ADDITIONAL EDGE PROPERTIES AT x/l_c = 0.5

(a) Wind tunnel

q_∞, kN/m^2	Test gas	p_l, kN/m^2	q_l, kN/m^2	u_l, m/sec	T_l, K
16.591	Air	14.240	42.589	866.55	437.56
94.918	Air	85.466	255.345	866.55	437.56
.807	Nitrogen	.728	2.480	1266.75	819.44
3.229	Nitrogen	2.820	9.619	1266.75	819.44
10.991	Helium	9.973	20.885	1671.22	320.33
1.055	Freon	.948	5.315	680.01	436.83
6.328	Freon	5.683	31.903	680.01	436.83

(b) Flight

q_∞, kN/m^2	State	p_l, kN/m^2	q_l, kN/m^2	u_l, m/sec	T_l, K
1.068	Equilibrium	0.905	7.723	5439.46	4651.67
2.639	Equilibrium	2.236	18.362	5435.19	4833.89
4.067	Equilibrium	3.457	25.439	4511.95	3980.56
2.603	Equilibrium	2.222	15.058	3598.47	2986.11
1.068	Nonequilibrium	.900	6.090	5407.46	6162.22
2.639	Nonequilibrium	2.207	11.960	5415.99	5770.00
4.067	Nonequilibrium	3.457	25.439	4511.95	3980.56
2.603	Nonequilibrium	2.222	15.058	3598.47	2986.11
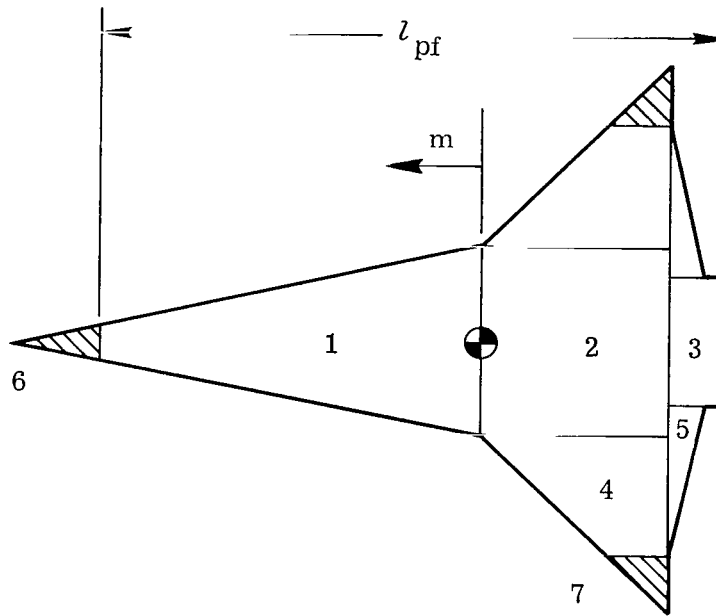
$$C_m = \frac{C_p \displaystyle\sum_{i=1}^{i=7} (A_{pf})_i\, m_i}{S_{pf}\, \ell_{rpf}}$$

A_{pf1} = 140.25 m_1 = 8.5   m   = Moment arm to center of gravity

A_{pf2} = 114.4 m_2 = -5.2 A_{tpf} = Total planform area = 396.31

A_{pf3} = 19.24 m_3 = -11.7 S_{pf} = Reference area = 271.4

A_{pf4} = 2 × 53.04 m_4 = -6.93 ℓ_{rpf} = Reference length = 38.6

A_{pf5} = 2 × 8.17 m_5 = -10.97

A_{pf6} = 4.8 m_6 = 22.4 $\displaystyle\sum_i (A_{pf})_i\, m_i$ = -539.93

A_{pf7} = 2 × 5.95 m_7 = -9.23

Figure 1.- Planform for estimating effect of lee-side pressure on orbiter pitching moment. Length in meters; area in m^2; planforms indicated by numbers.
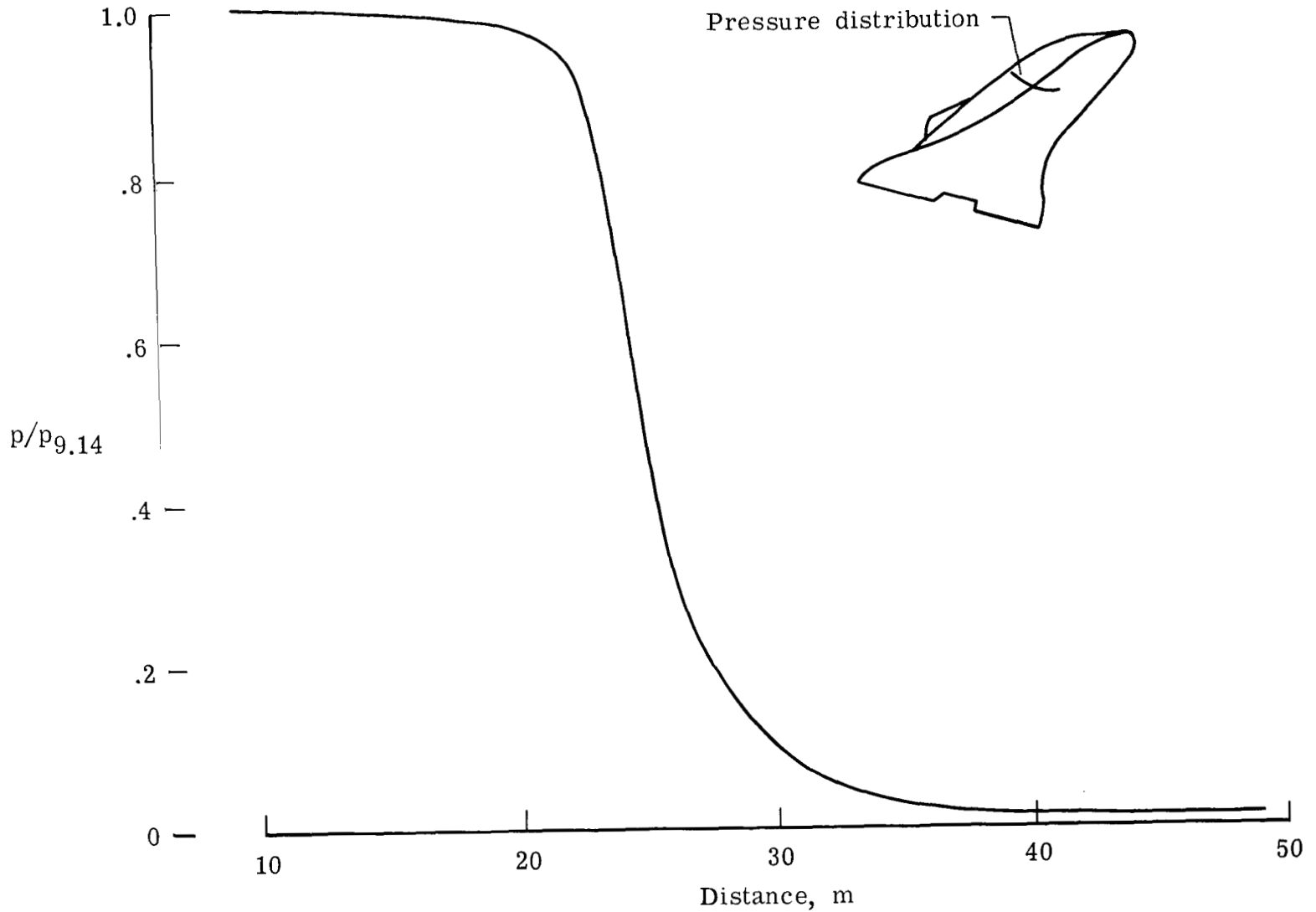
Figure 2.- Streamline pressure distribution for orbiter configuration starting on center line at 9.14 m from nose. $\alpha = 20°$; $u_\infty = 6096$ m/sec; Altitude = 67 056 m; $p_2 = (3.9 \text{ kPa} \times 10^{-2} \text{ atm})$; $p_\infty = (0.095 \text{ kPa} \times 10^{-4} \text{ atm})$.
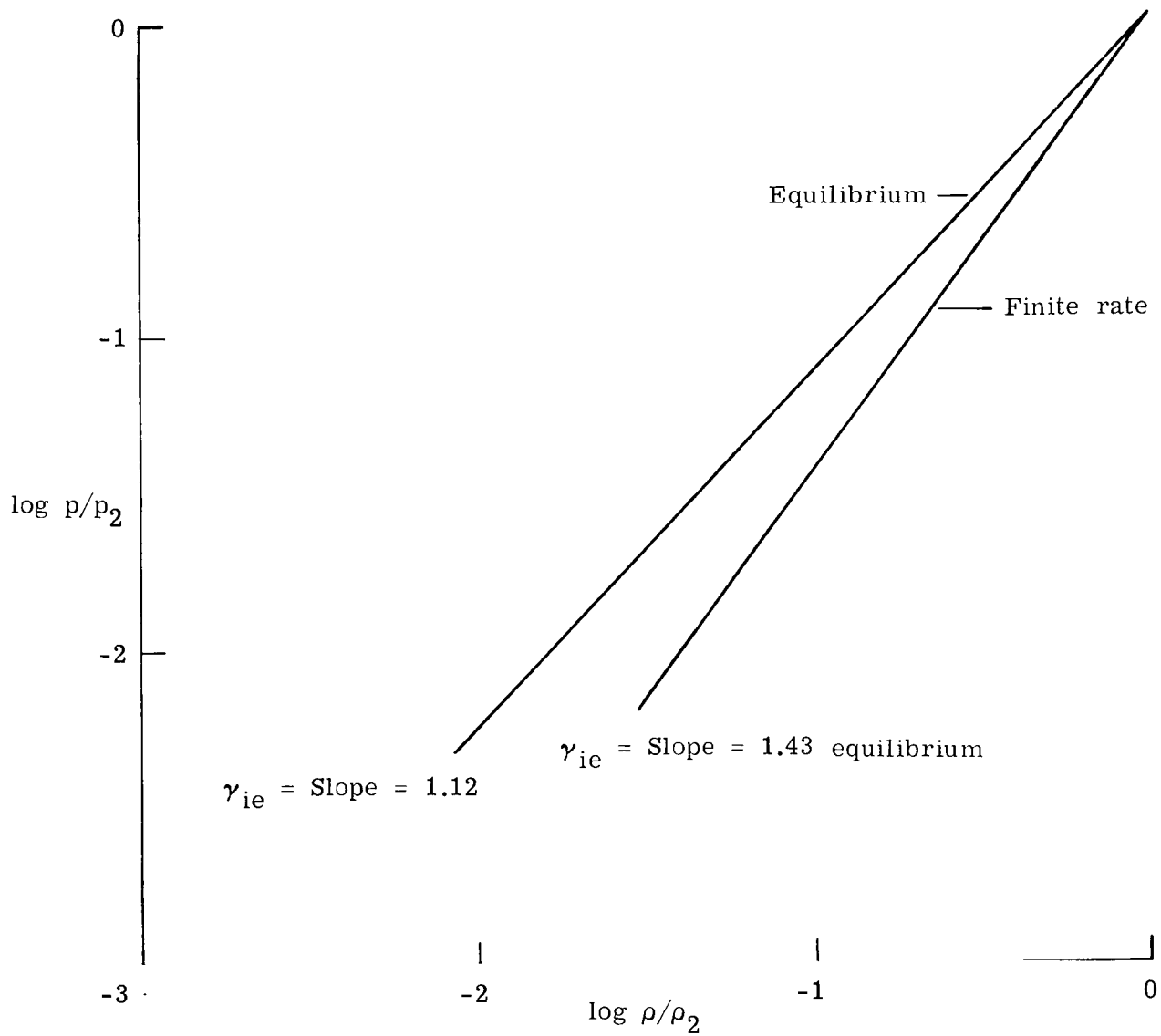
Figure 3.- Isentropic exponent in expansion to leeward side.
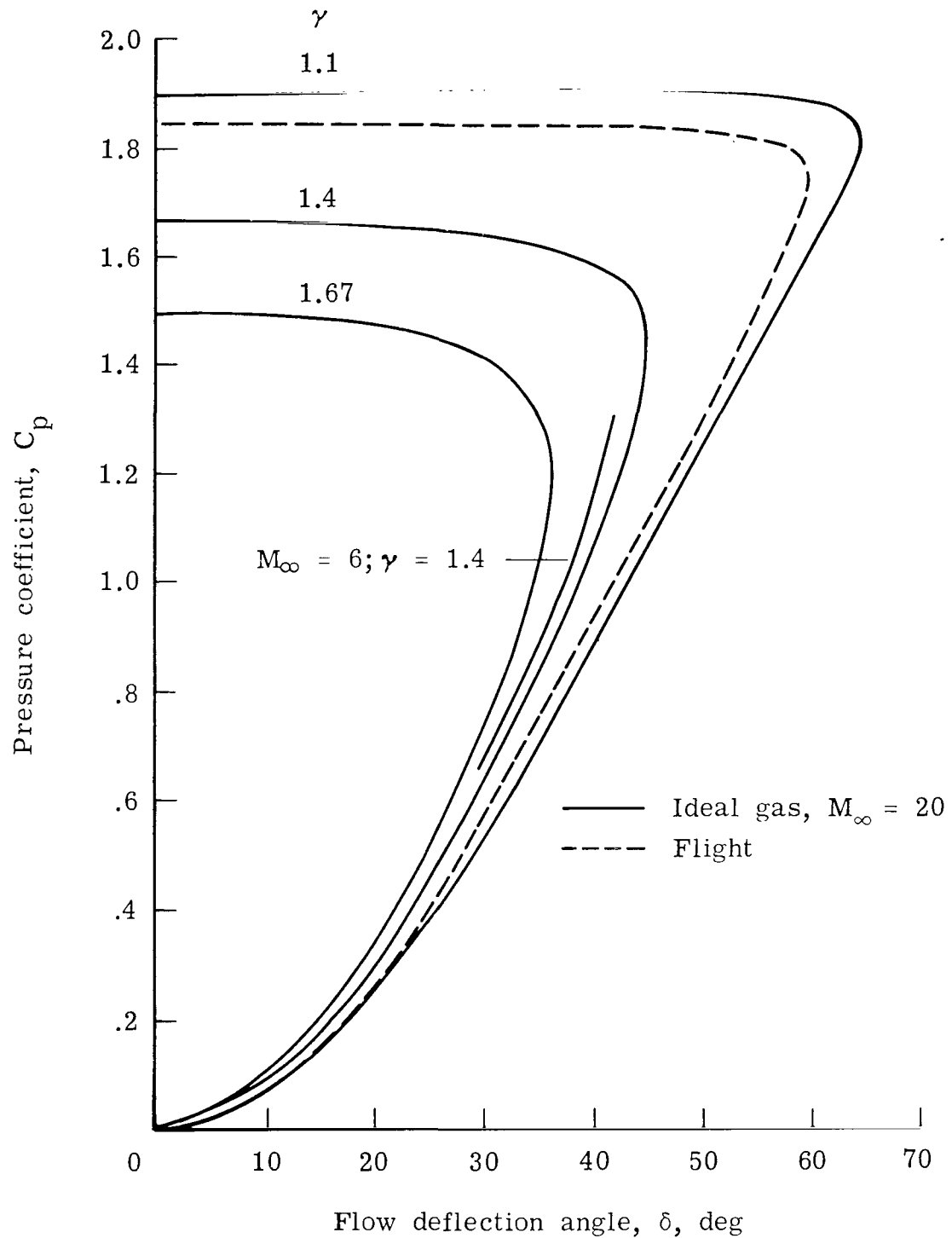
Figure 4.- Variation of pressure coefficient with flow deflection angle. Velocity, 6096 m/sec; altitude, 60 964 m.
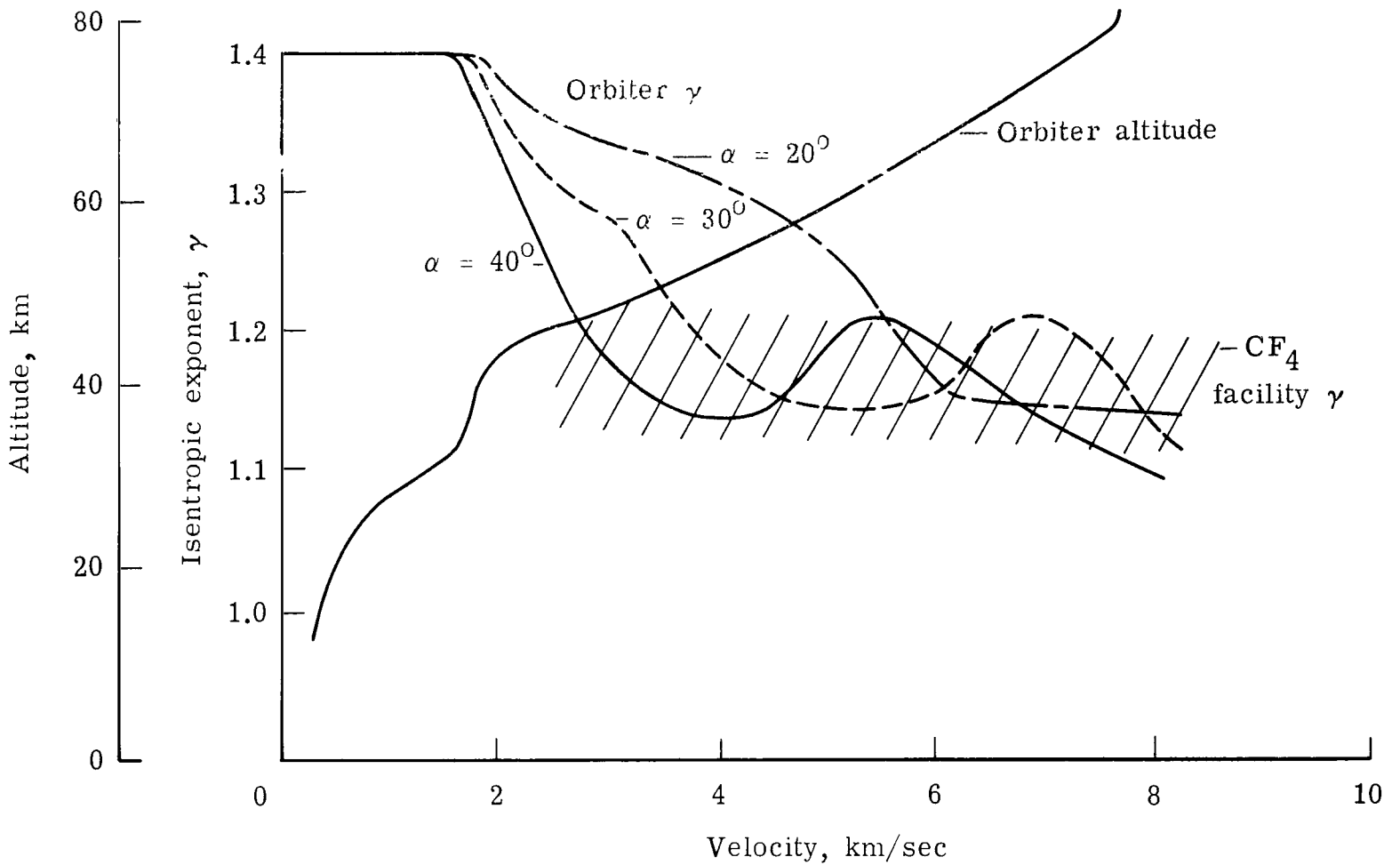
Figure 5.- Oblique shock isentropic exponent for shuttle entry at $\alpha = 20^o$, 30°, and 40°.
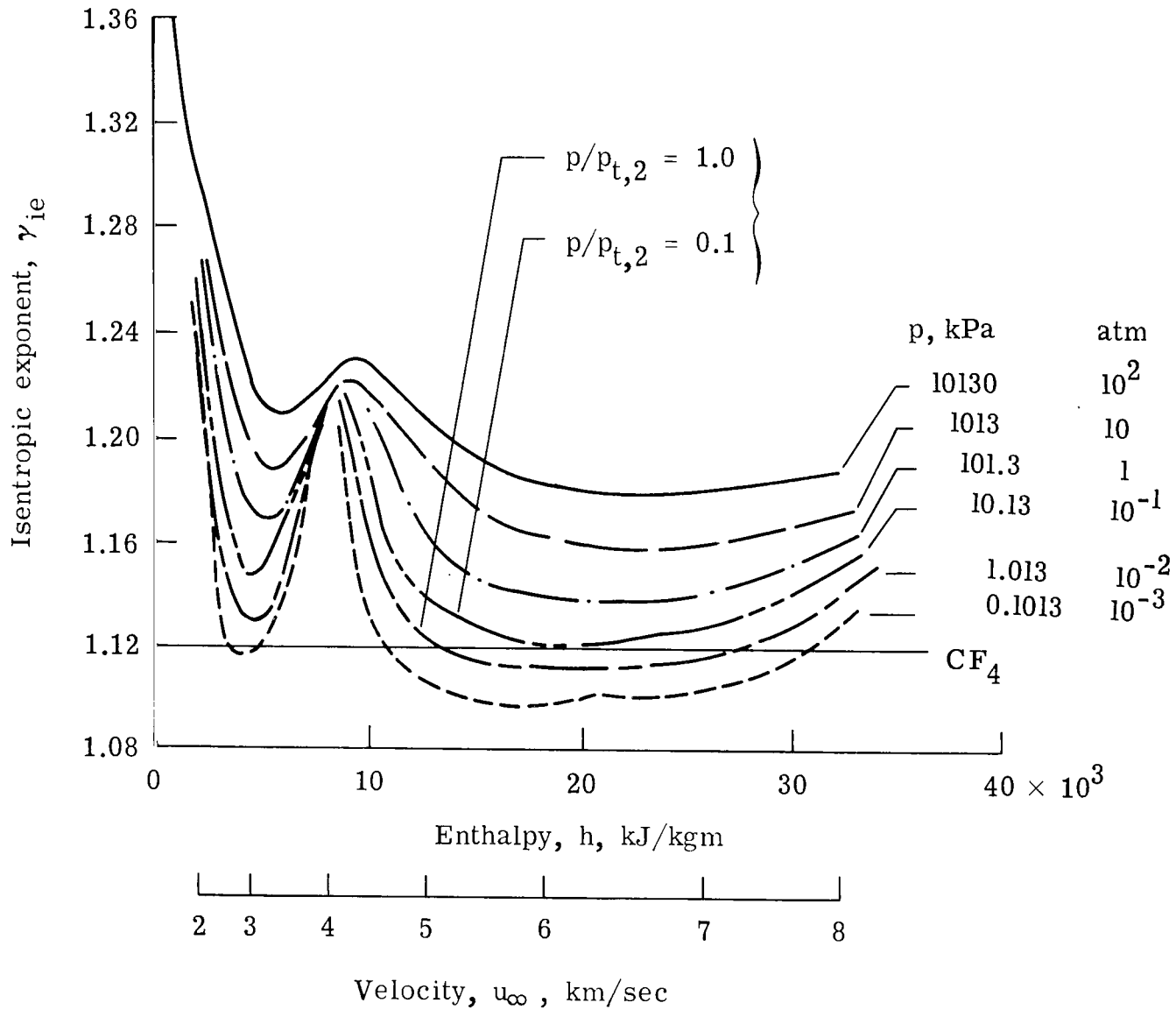
Figure 6.- Isentropic exponent for air. Altitude, 60 960 m, velocity, 6705.6 m/sec.
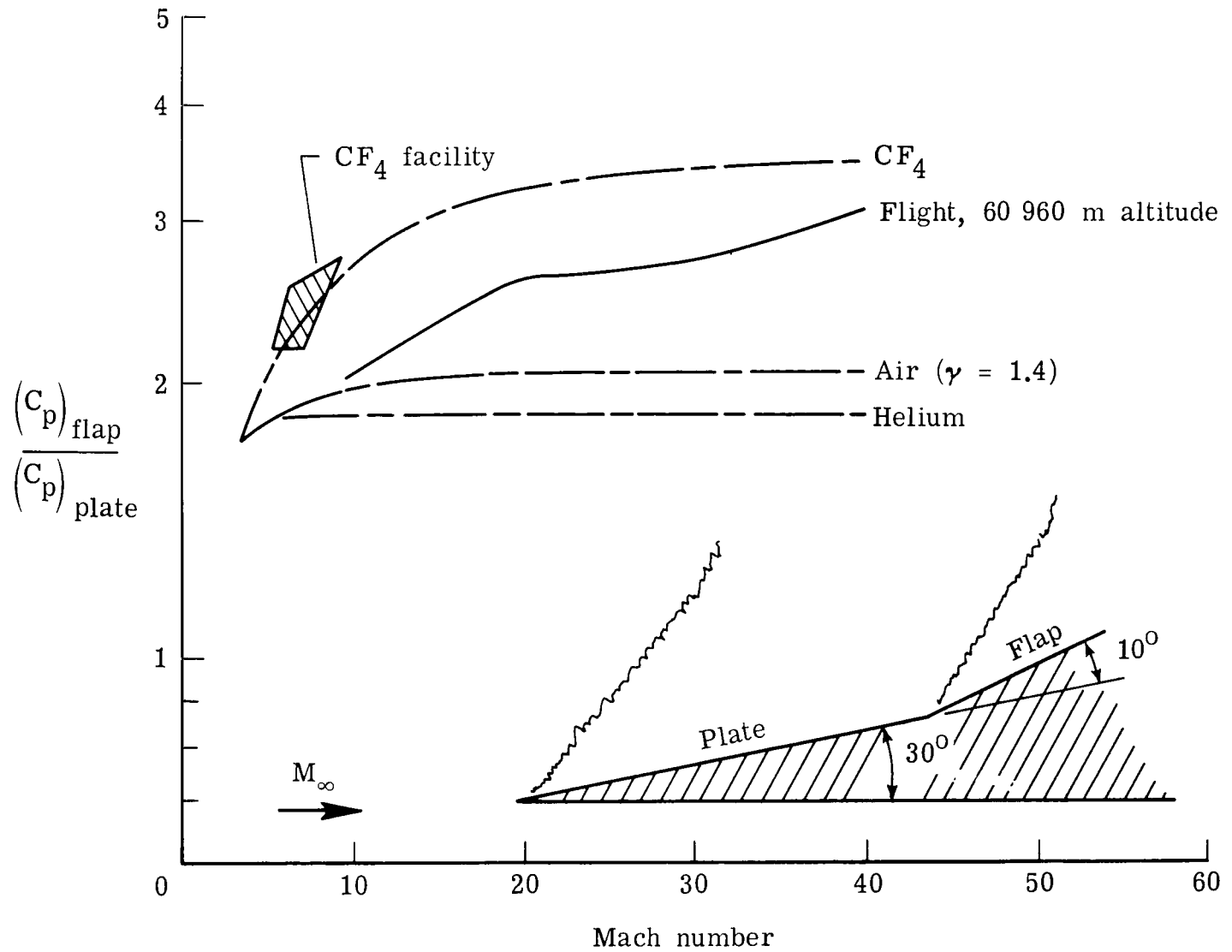
Figure 7.- Real-gas effect on flap effectiveness.

2×10^4

CF$_4$, M = 6

Ideal air, M = 19

Helium, M = 20

Flight: 6.1 km/sec, velocity
61.0 km, altitude

C_m

45.7 m 6.1 m 10°

1×10^4

δ

Moment center

0

10   20   30   40   50

α, deg
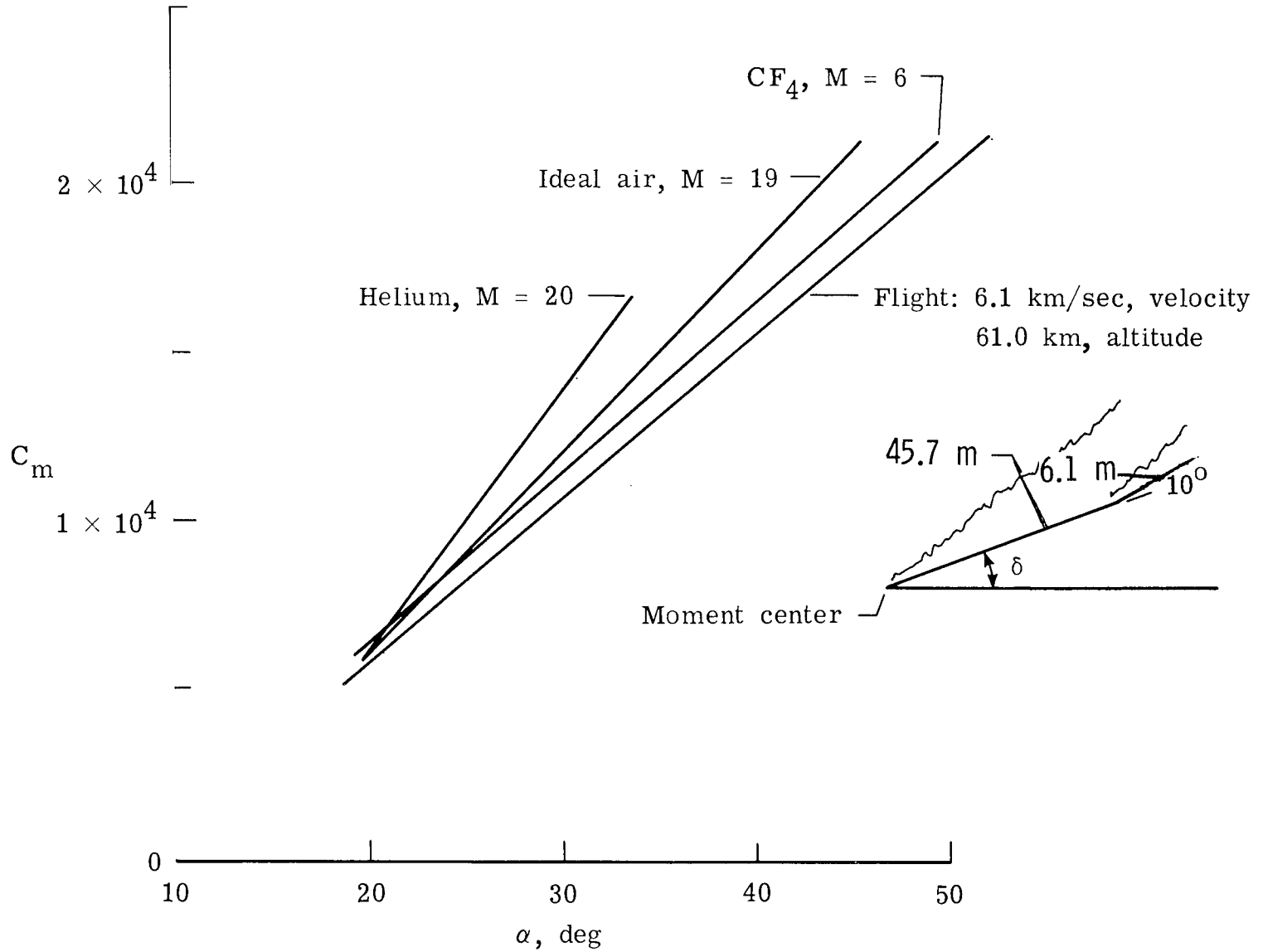
Figure 8.- Real-gas effect on pitching-moment coefficient.
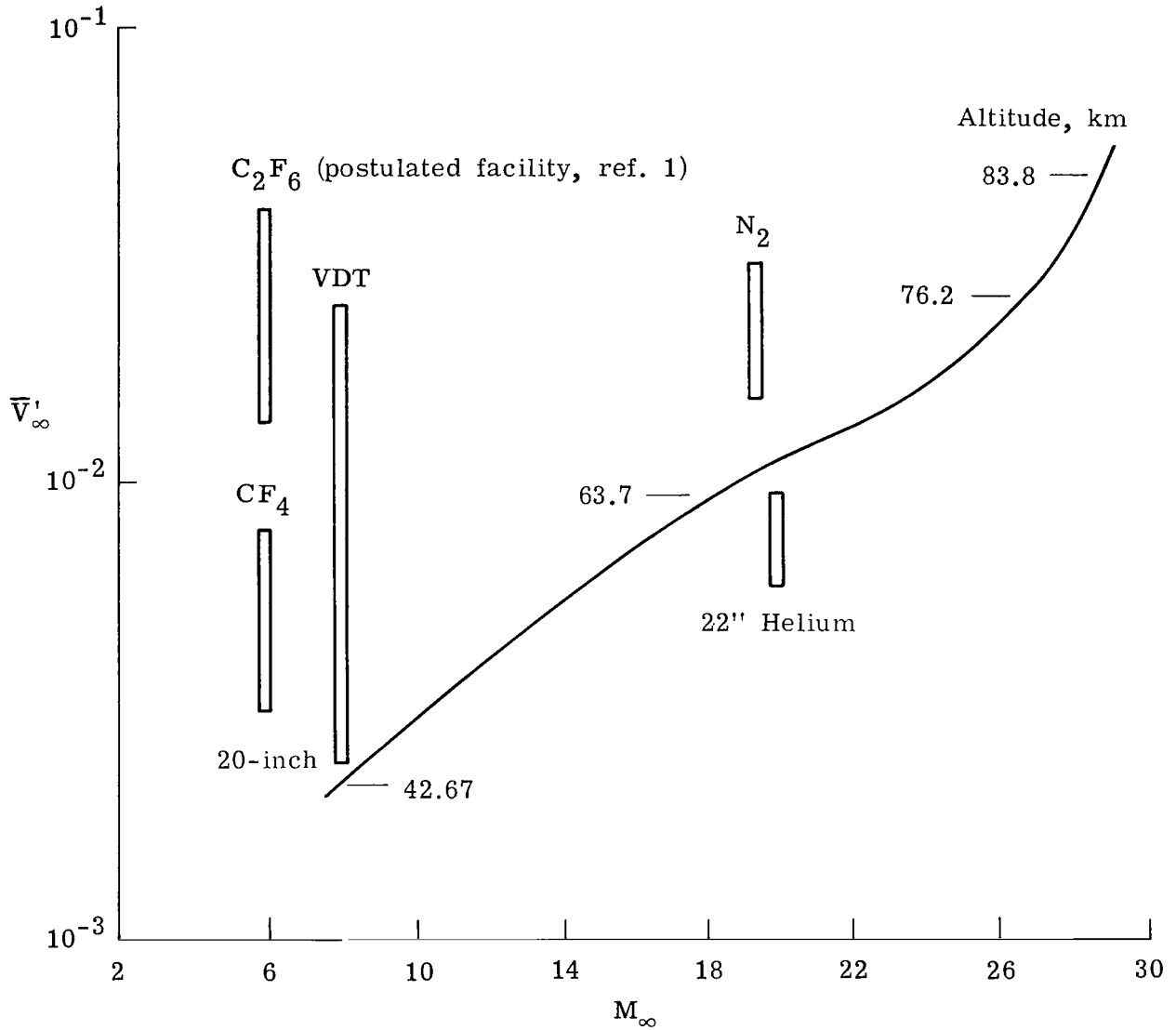
Figure 9.- Hypersonic viscous interaction parameter as function of Mach number for shuttle trajectory and Langley facilities. (Model length is tailored to given facility.)
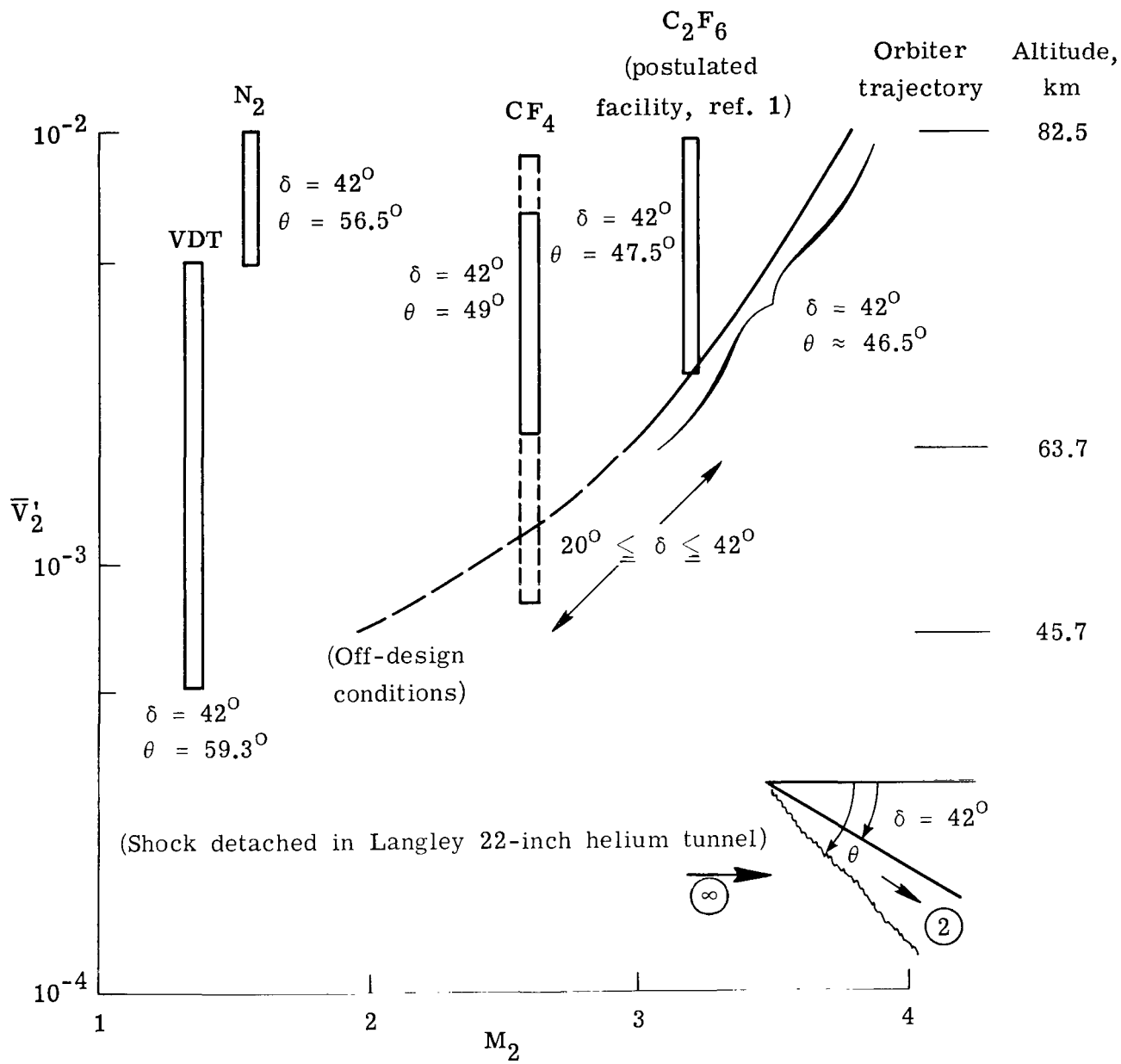
Figure 10.- Hypersonic viscous interaction parameter behind wedge shock as function of Mach number behind wedge shock for shuttle trajectory and Langley facilities.
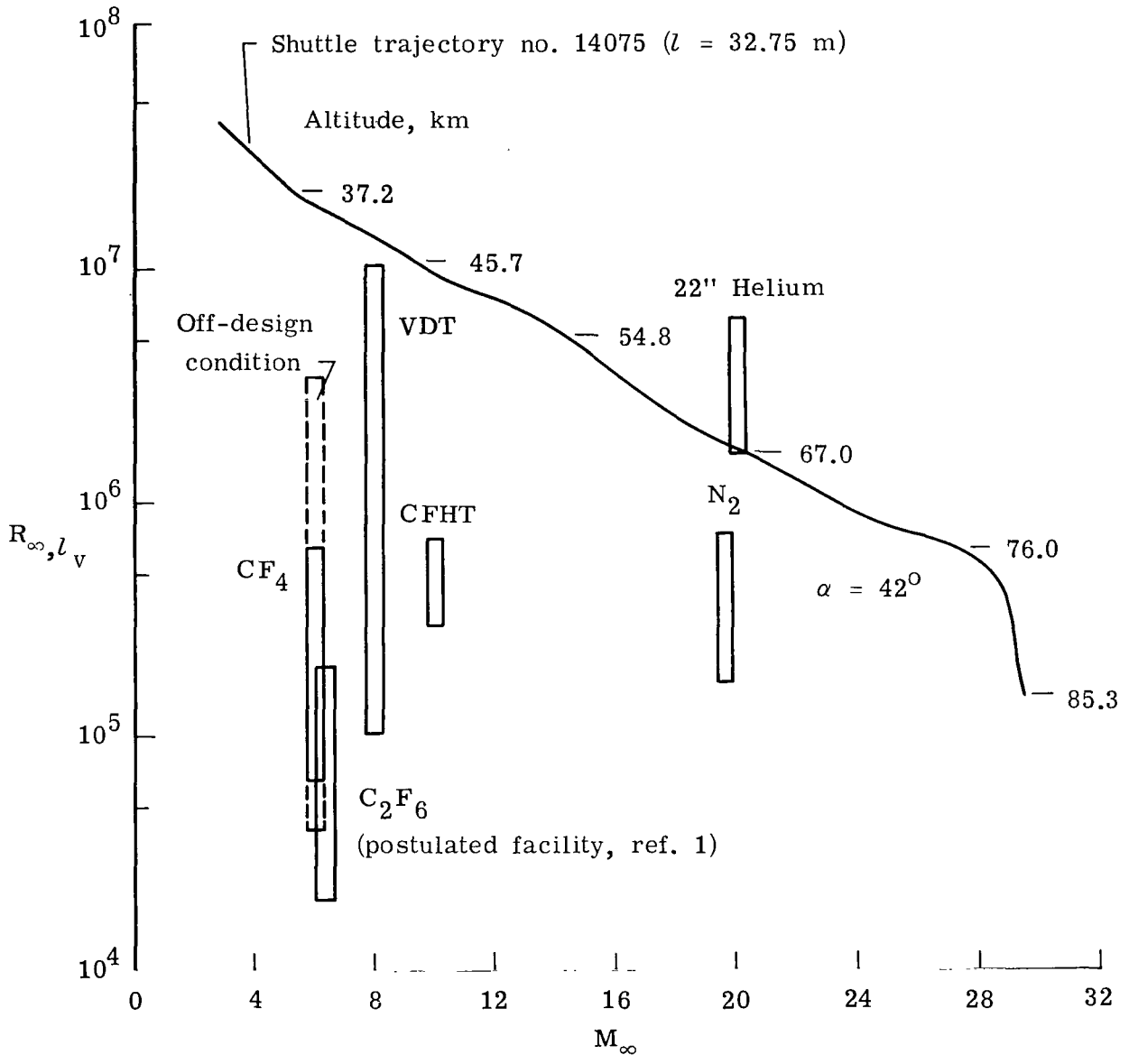
Figure 11.- Reynolds number as function of stream Mach number for shuttle trajectory and Langley hypersonic facilities.
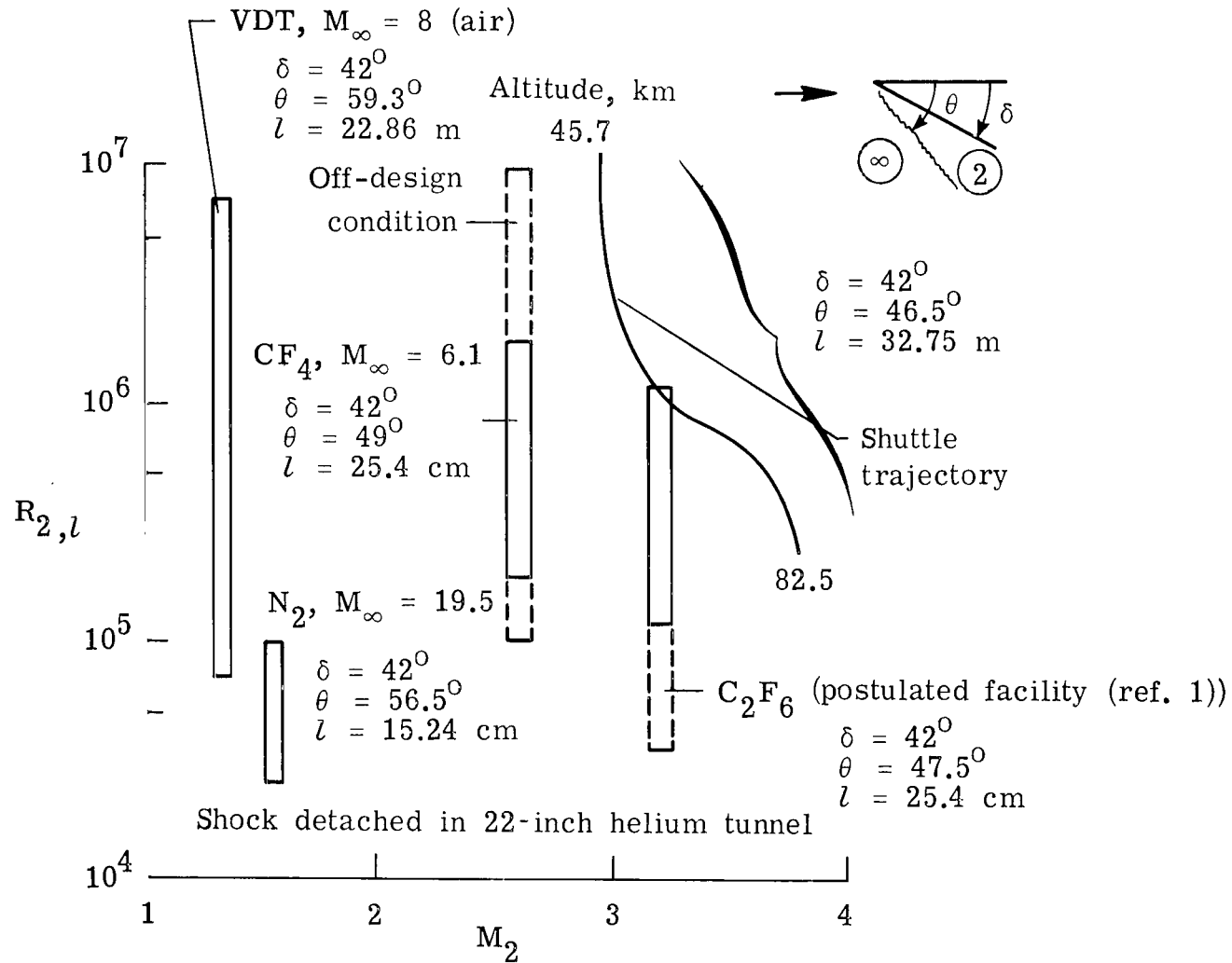
Figure 12.- Reynolds number behind wedge shock as function of Mach number behind wedge shock for shuttle trajectory (α = 42° position) and Langley hypersonic facilities.
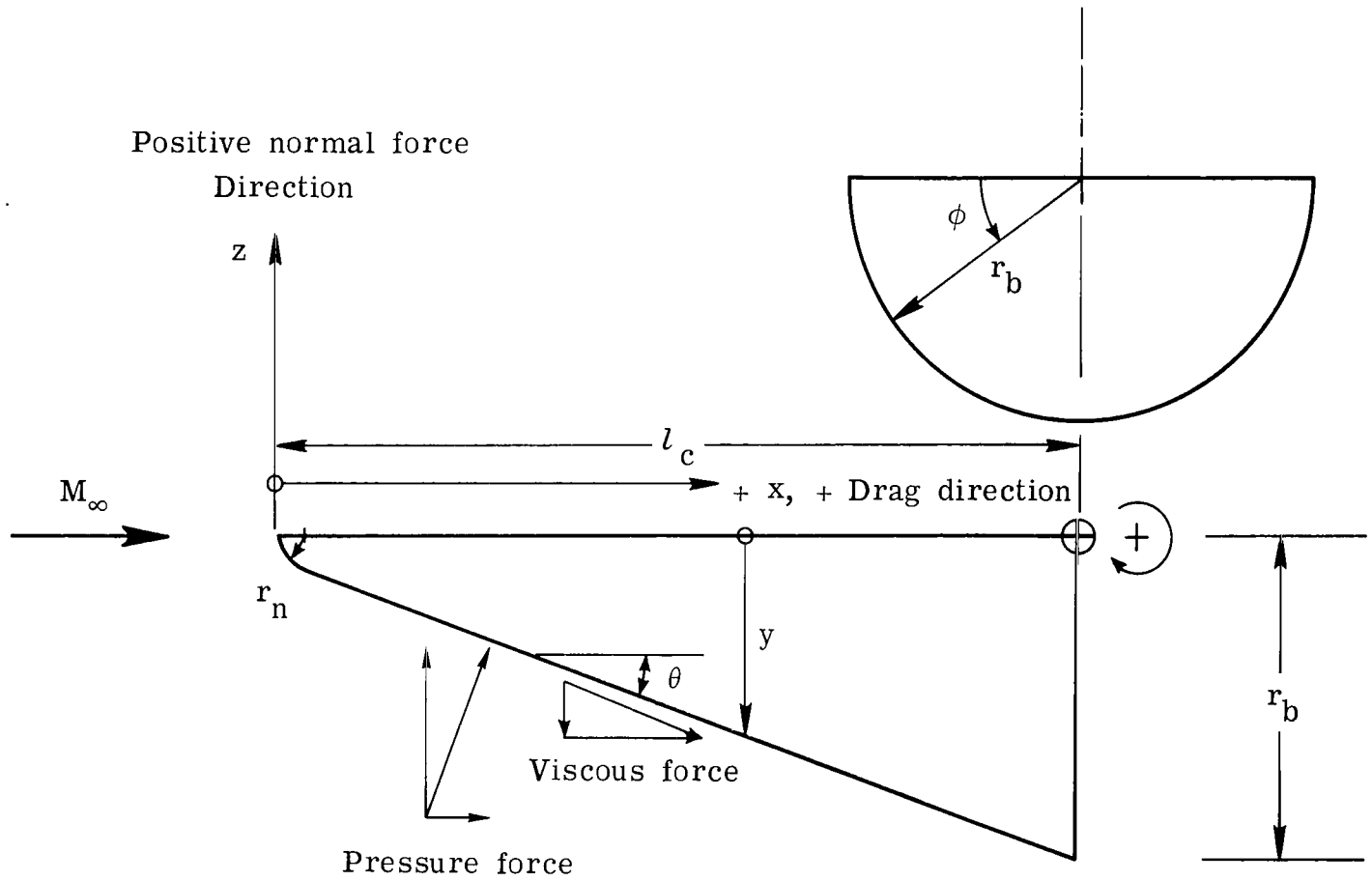
Figure 13.- Half-cone model. $\iota/r_n = 50$; $\theta = 40^o$.
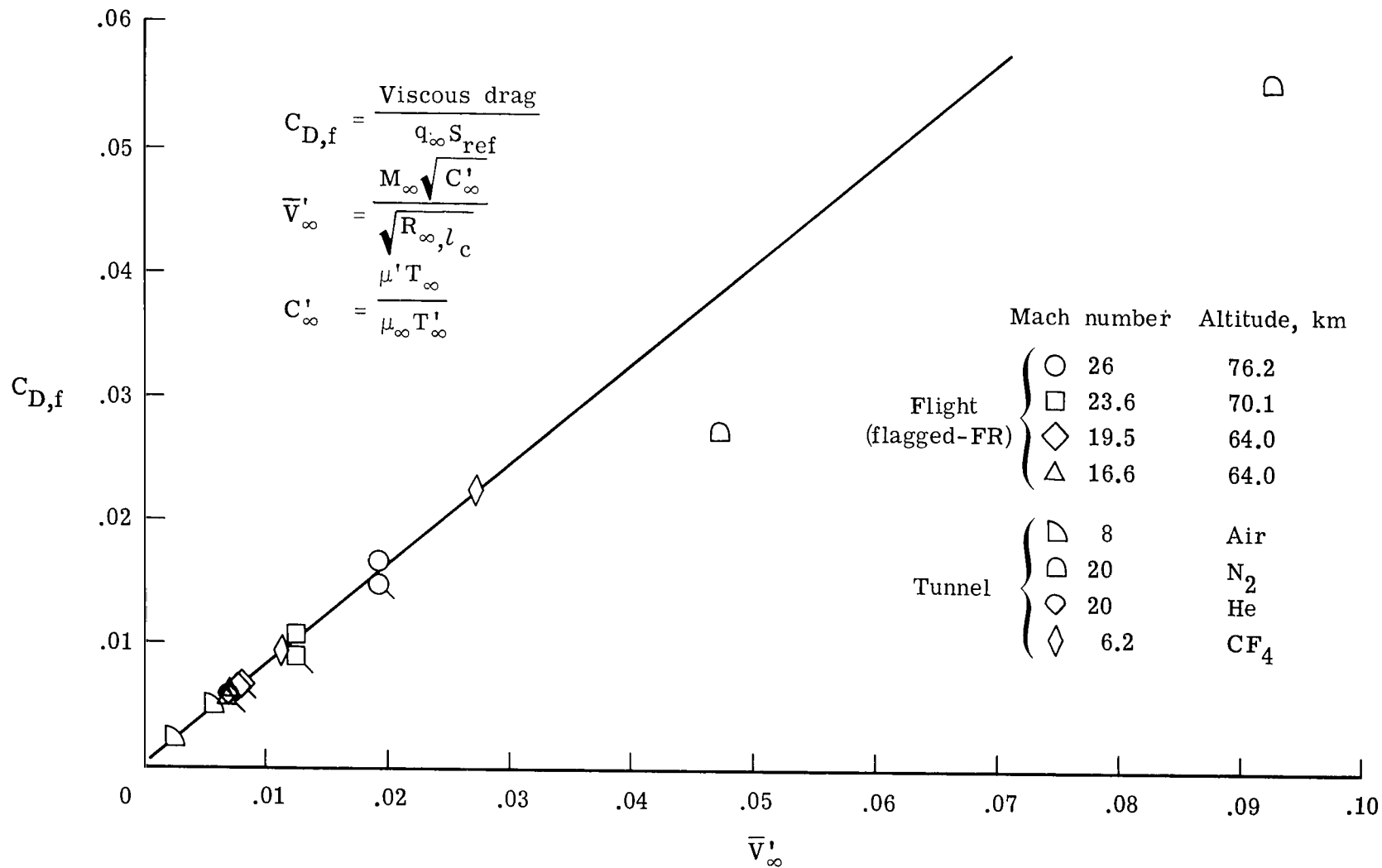
Figure 14.- Viscous drag coefficient as function of interaction parameter
based on free-stream conditions.
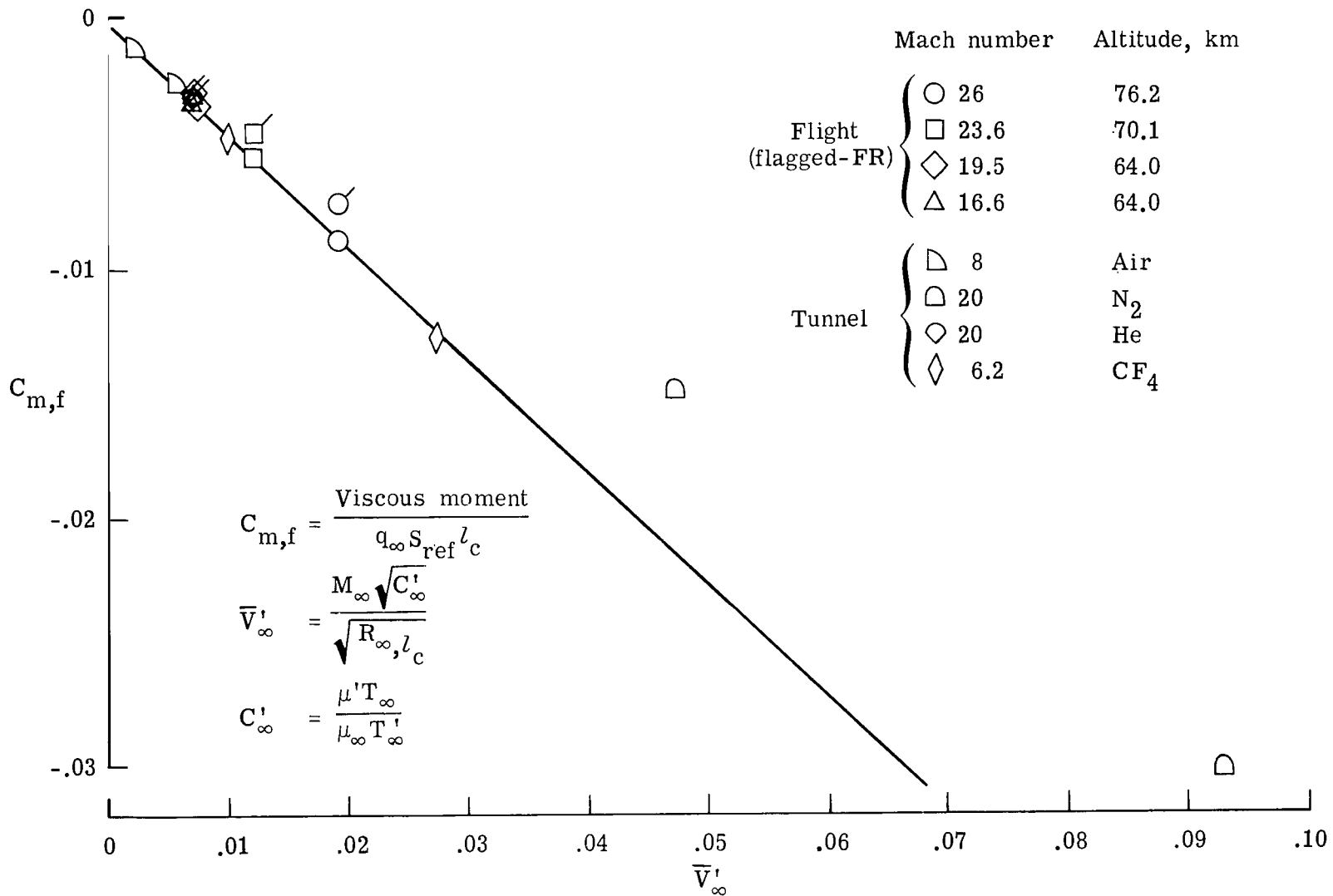
Figure 15.- Viscous pitching-moment coefficient as function of viscous interaction
parameter based on free-stream conditions.

Legend:

	Mach number	Altitude, km
Flight (flagged-FR) ⟨ ○	26	76.2
□	23.6	70.1
◇	19.5	64.0
△	16.6	64.0
Tunnel ⟨ ◠	8	Air
◠	20	N_2
◠	20	He
◇	6.2	CF_4

$$C_{m,f} = \frac{\text{Viscous moment}}{q_\infty S_{ref} l_c}$$

$$\overline{V}'_\infty = \frac{M_\infty \sqrt{C'_\infty}}{\sqrt{R_{\infty, l_c}}}$$

$$C'_\infty = \frac{\mu' T_\infty}{\mu_\infty T'_\infty}$$
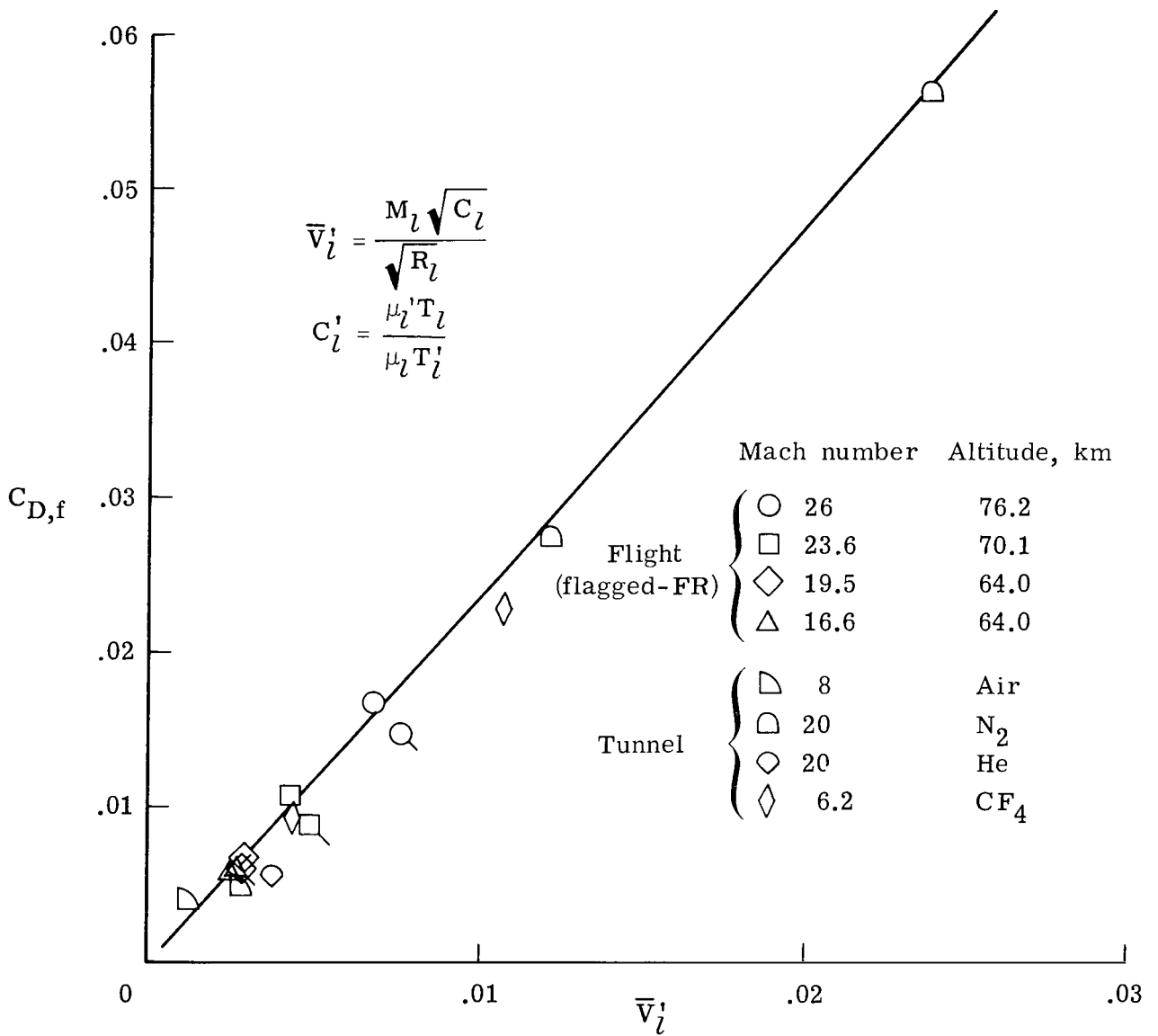
Figure 16.- Viscous drag coefficient as function of viscous interaction parameter based on local conditions at $x/l_c = 0.5$.
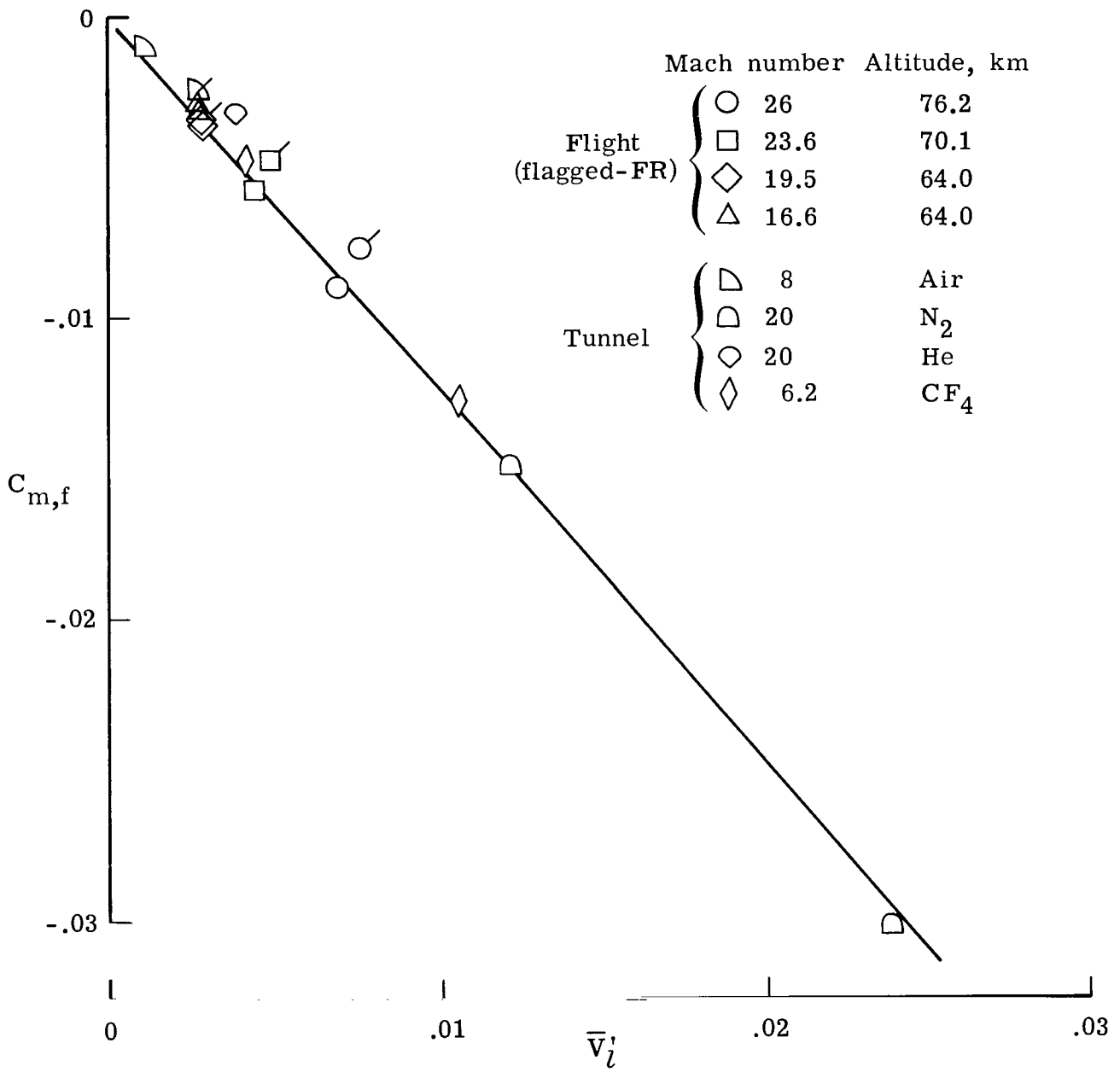
Figure 17.- Viscous pitching moment as function of viscous interaction parameter based on local conditions at $x/l_c = 0.5$.
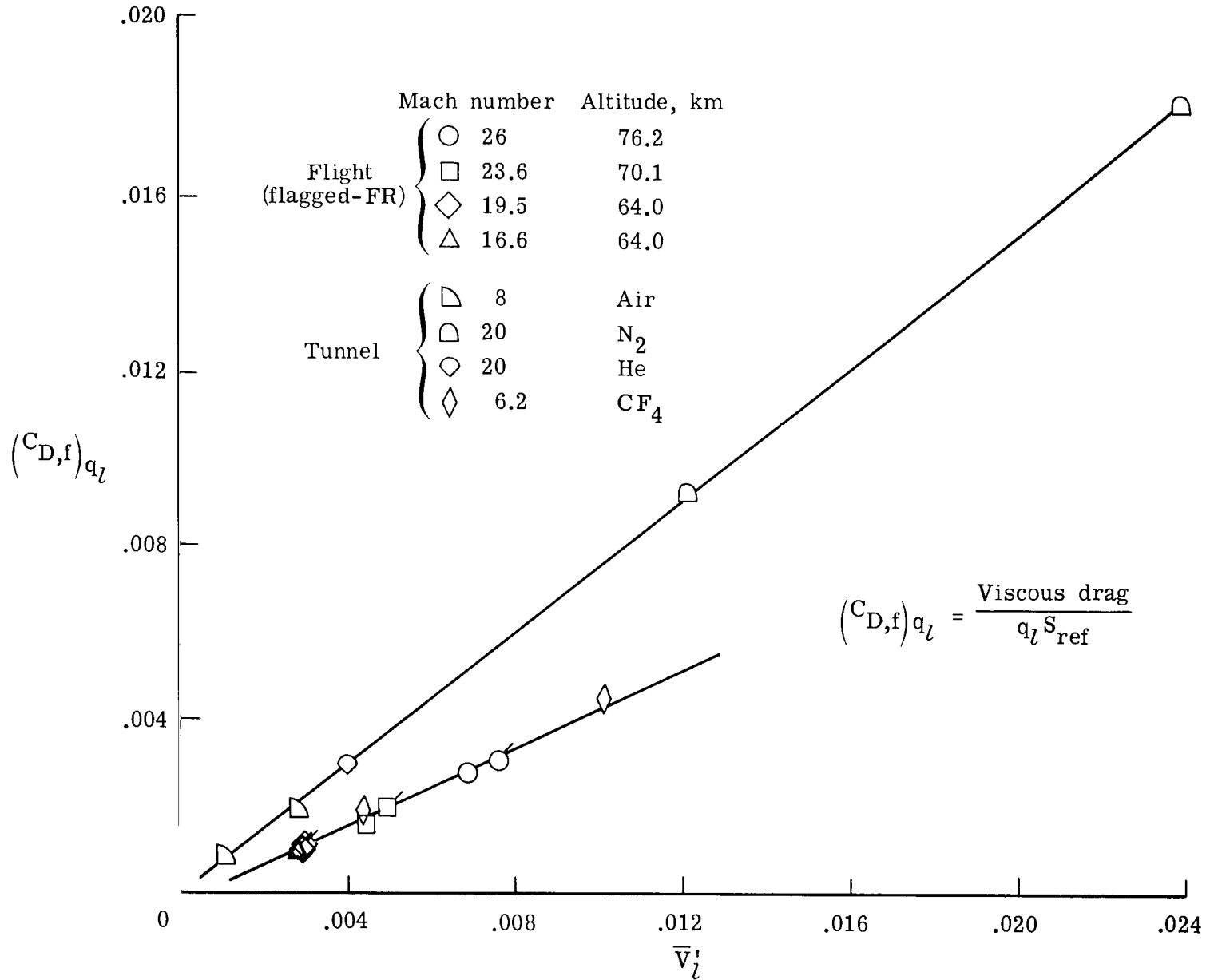
Figure 18.- Viscous drag coefficient nondimensionalized by local dynamic pressure as function of viscous interaction parameter based on local conditions at $x/l_c = 0.5$.
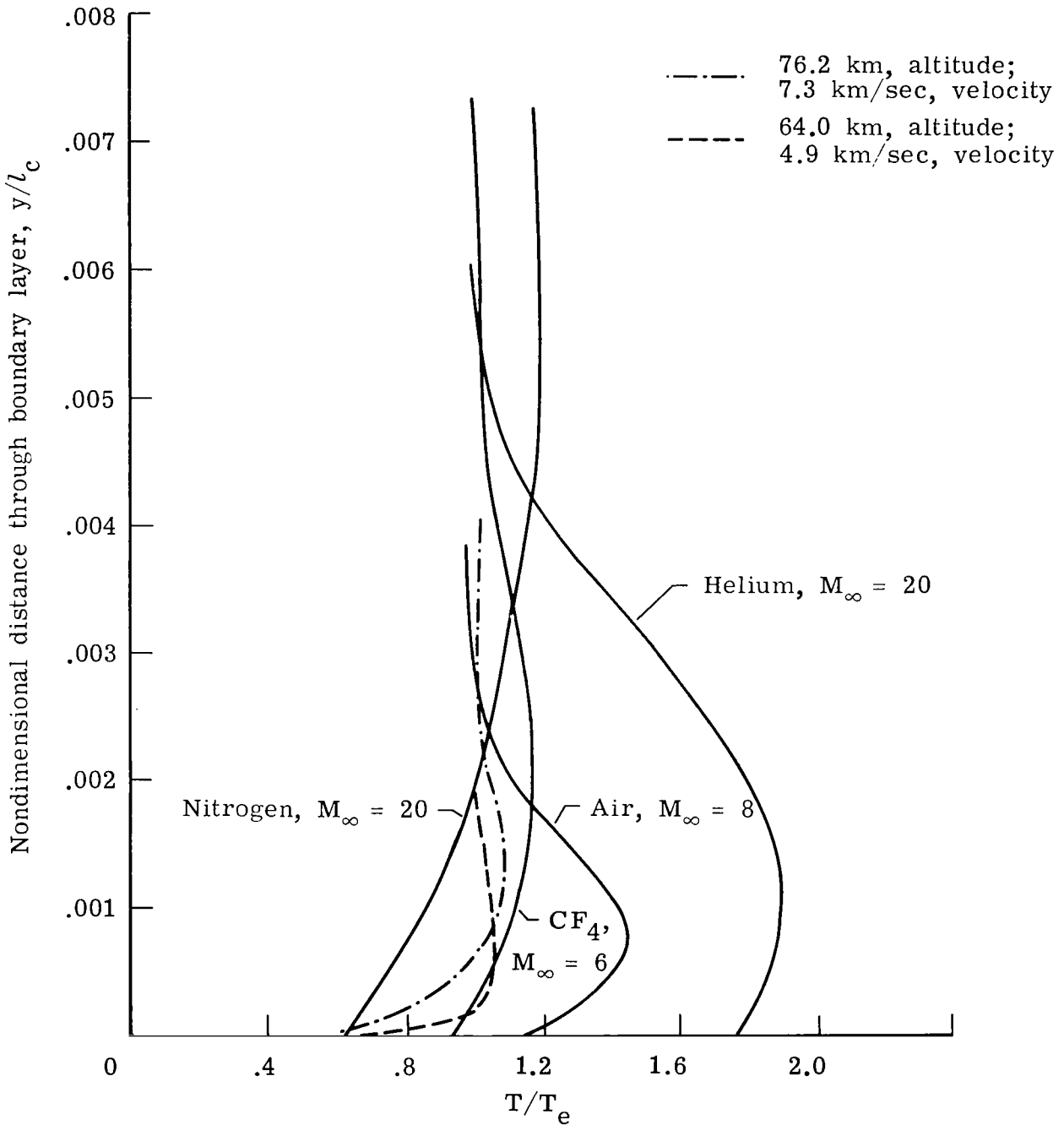
Figure 19.- Boundary-layer temperature profiles. Laminar flow; 0.524 radius cone; $l_c/r_n = 100$; $l/l_c = 0.65$.
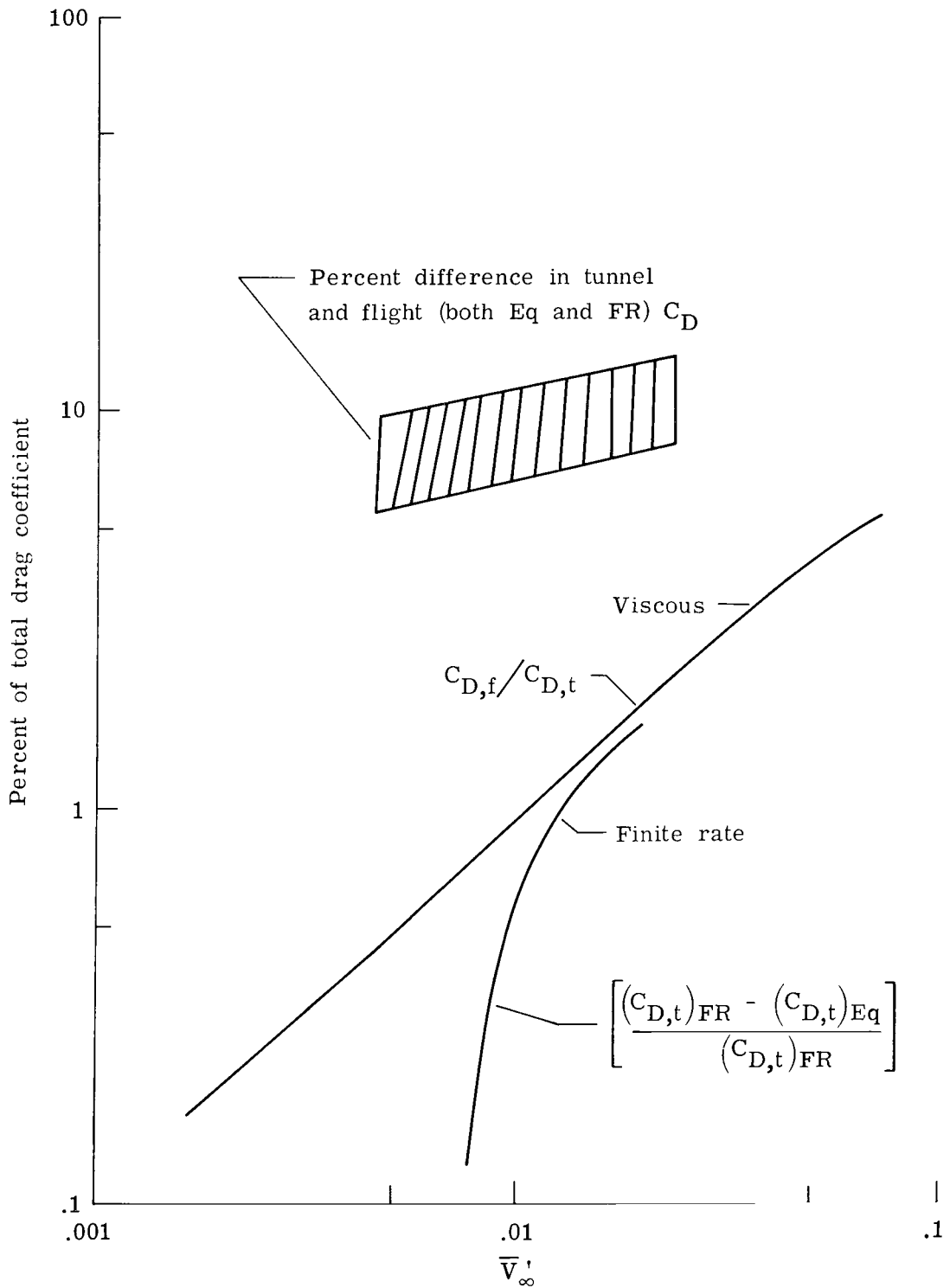
Figure 20.- Relative contribution of phenomena influencing drag coefficient.
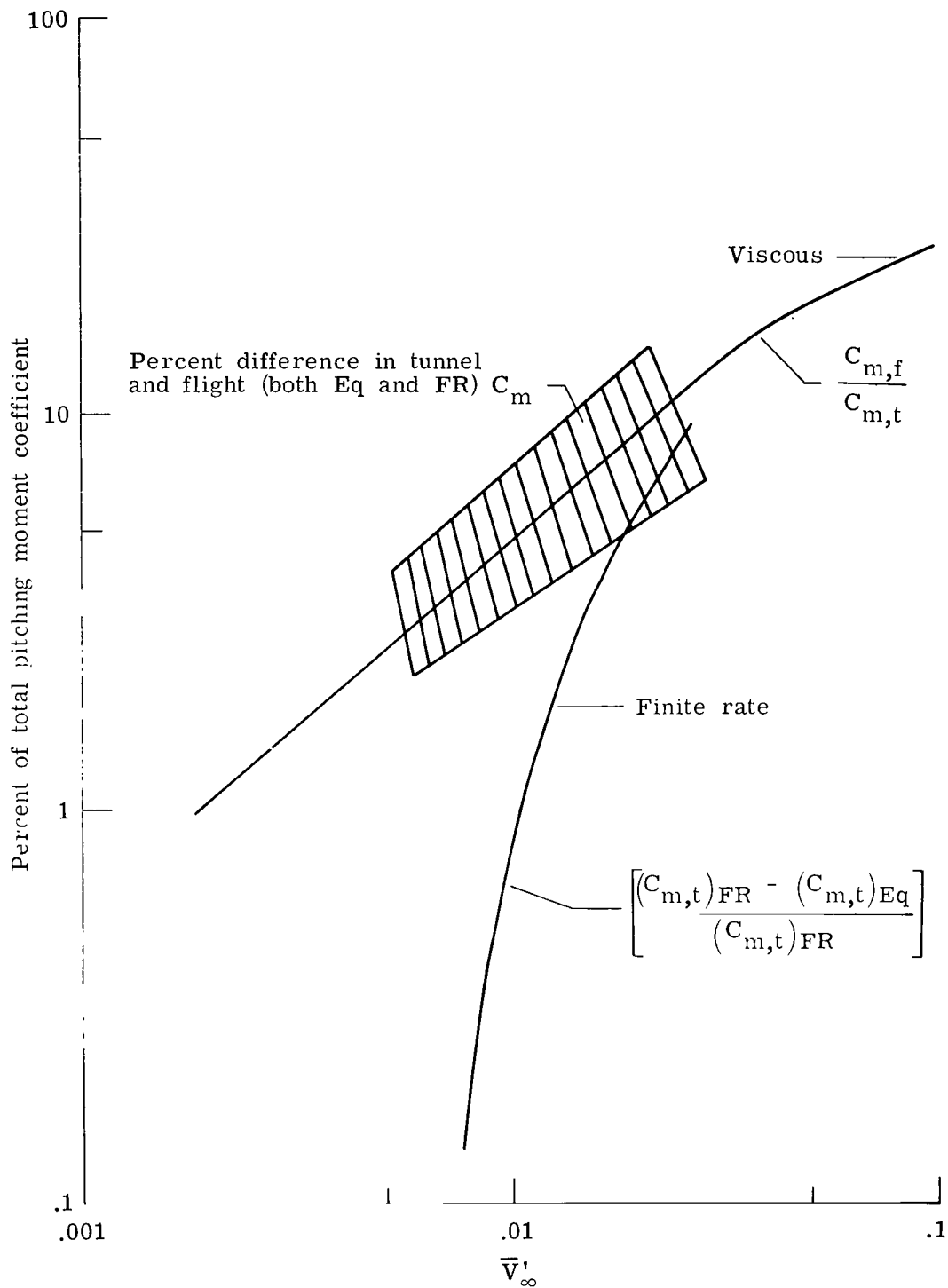
Figure 21.- Relative contribution of phenomena influencing pitching-moment coefficient.
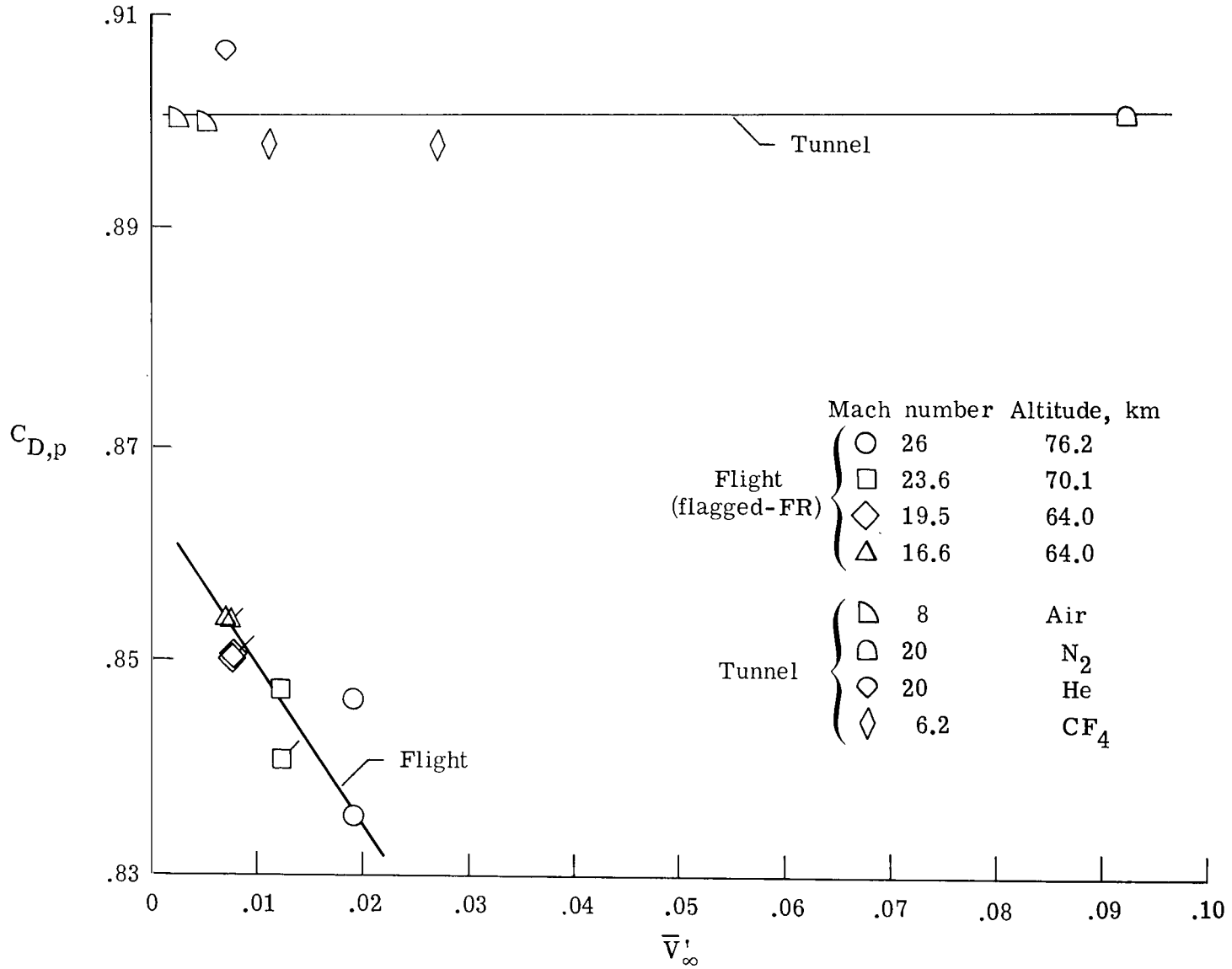
Figure 22.- Inviscid drag coefficient on 40° half-angle cone (obtained with partially coupled inviscid-viscid real-gas solution).
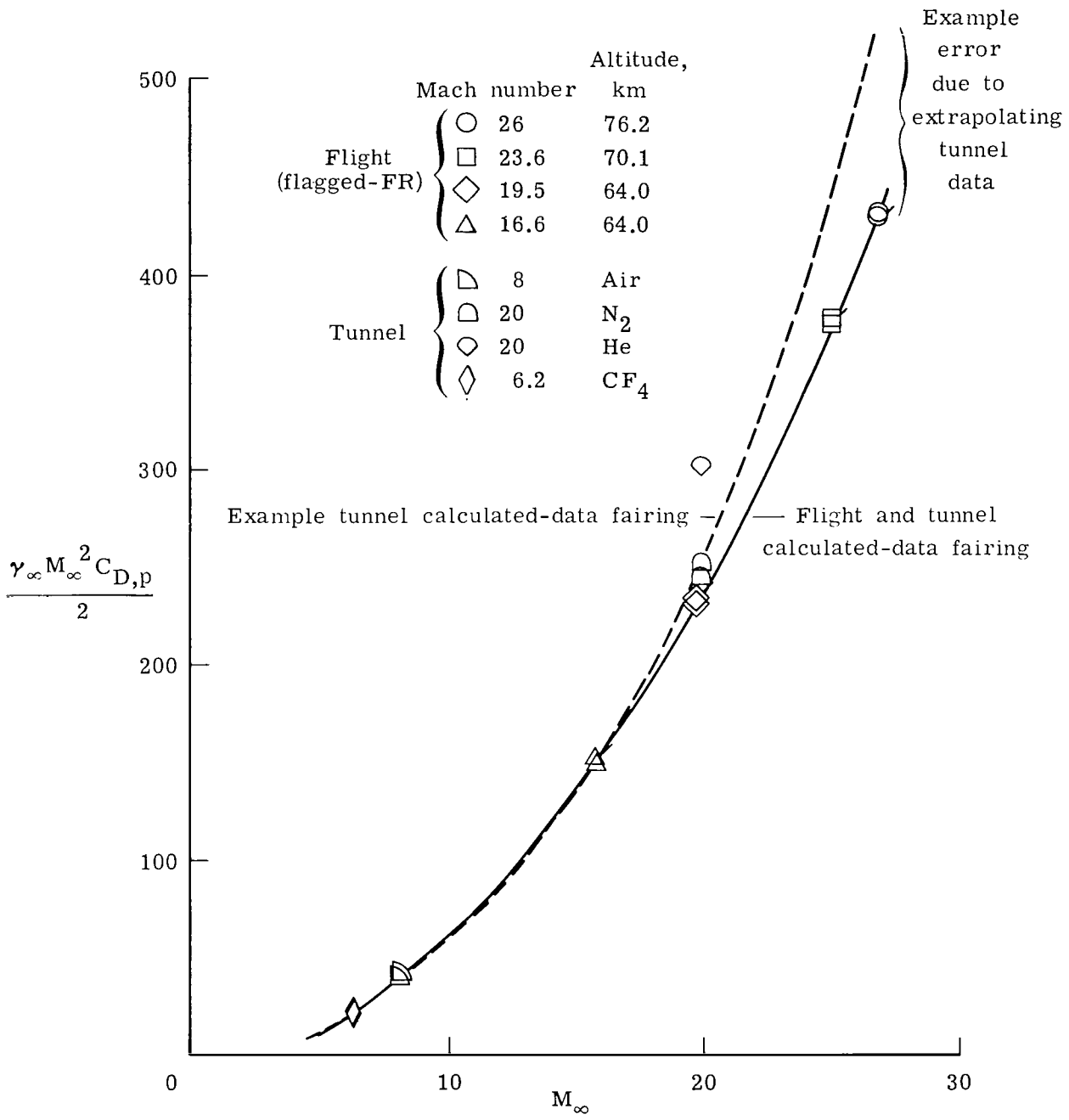
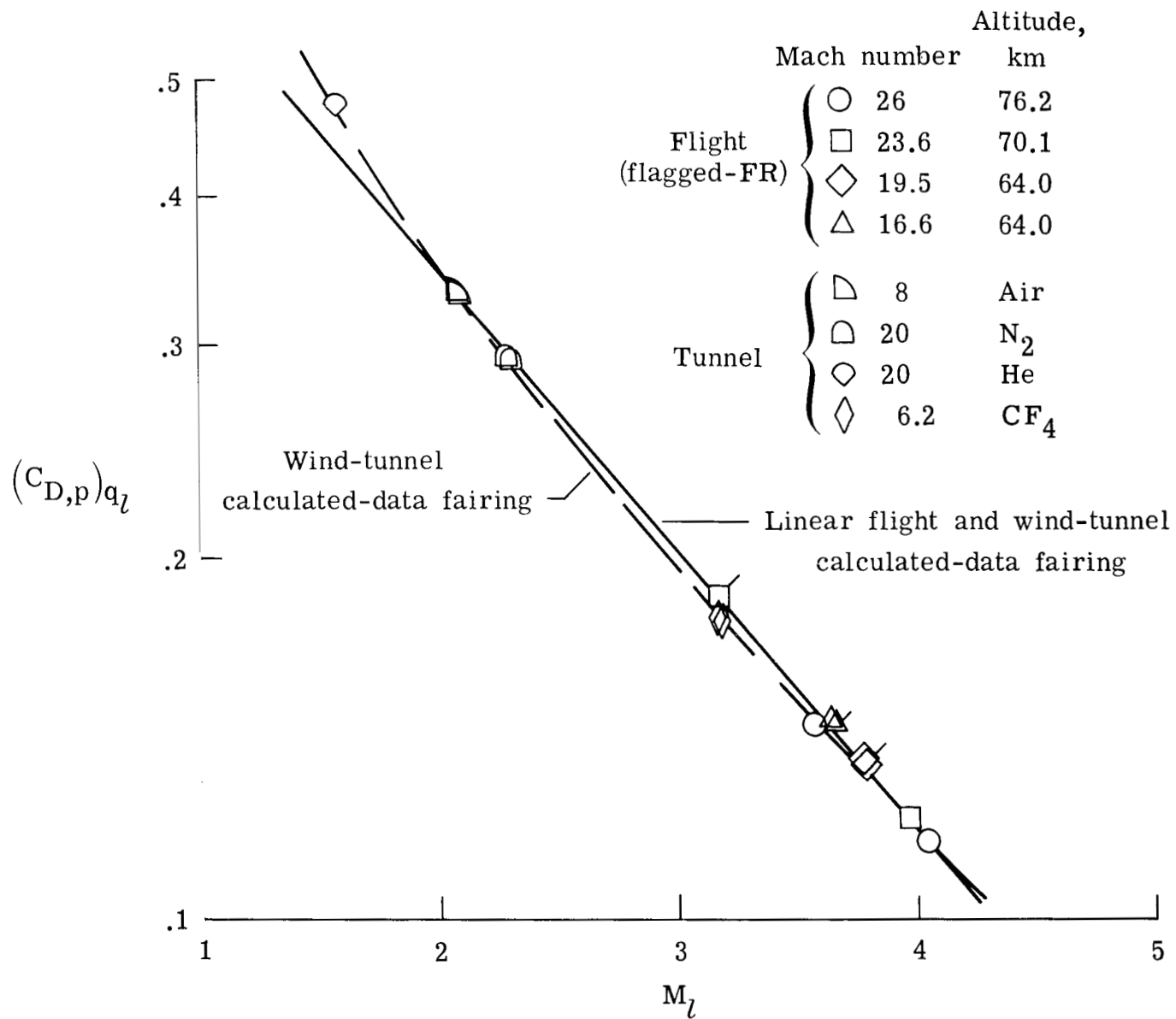Figure 23.- Hypersonic similarity approach to correlating pressure drag.

	Mach number	Altitude, km
Flight (flagged-FR)	○ 26	76.2
	□ 23.6	70.1
	◇ 19.5	64.0
	△ 16.6	64.0
Tunnel	⌂ 8	Air
	⌂ 20	N_2
	◇ 20	He
	◇ 6.2	CF_4

$(C_{D,p})q_l$

Wind-tunnel calculated-data fairing

Linear flight and wind-tunnel calculated-data fairing

M_l

Figure 24.- Inviscid correlation of pressure drag coefficient based on local conditions.
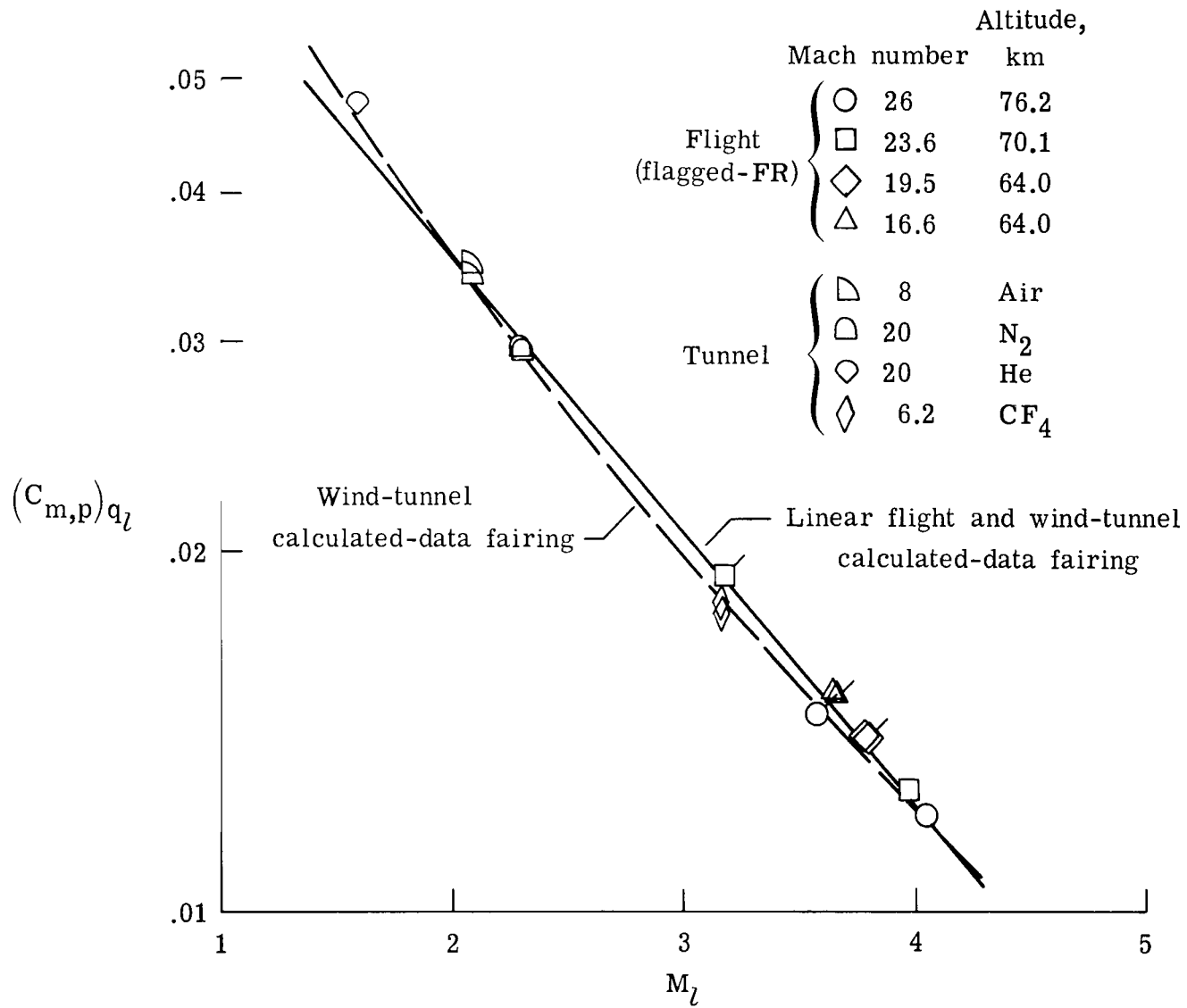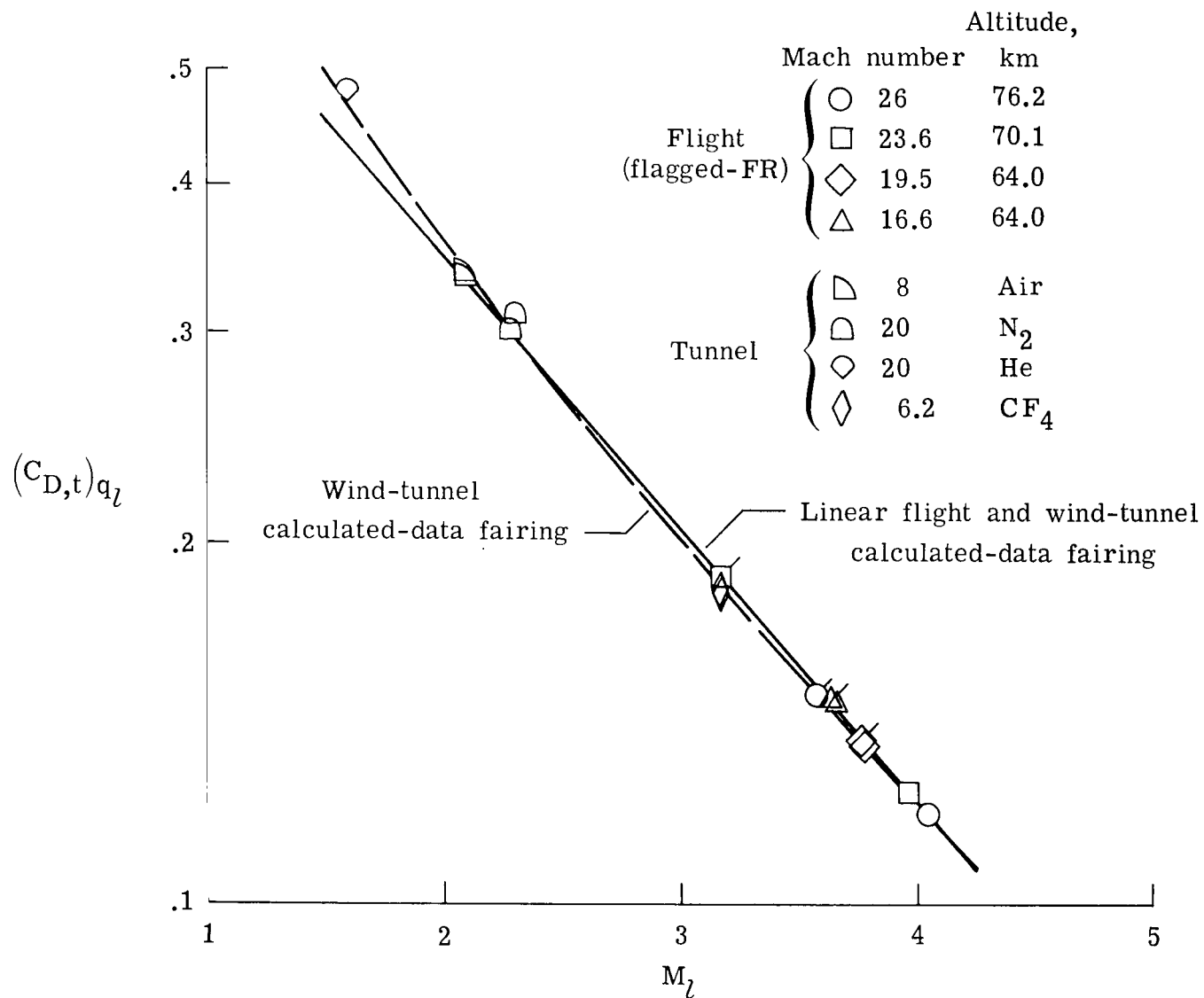
Figure 25.- Inviscid correlation of pitching-moment coefficient based on local conditions.

Figure 26.- Correlation of total drag coefficient (nondimensionalized by local dynamic pressure) with local Mach number. Real-gas effects correlate best in terms of M_l with coefficients nondimensionalized by q_l.
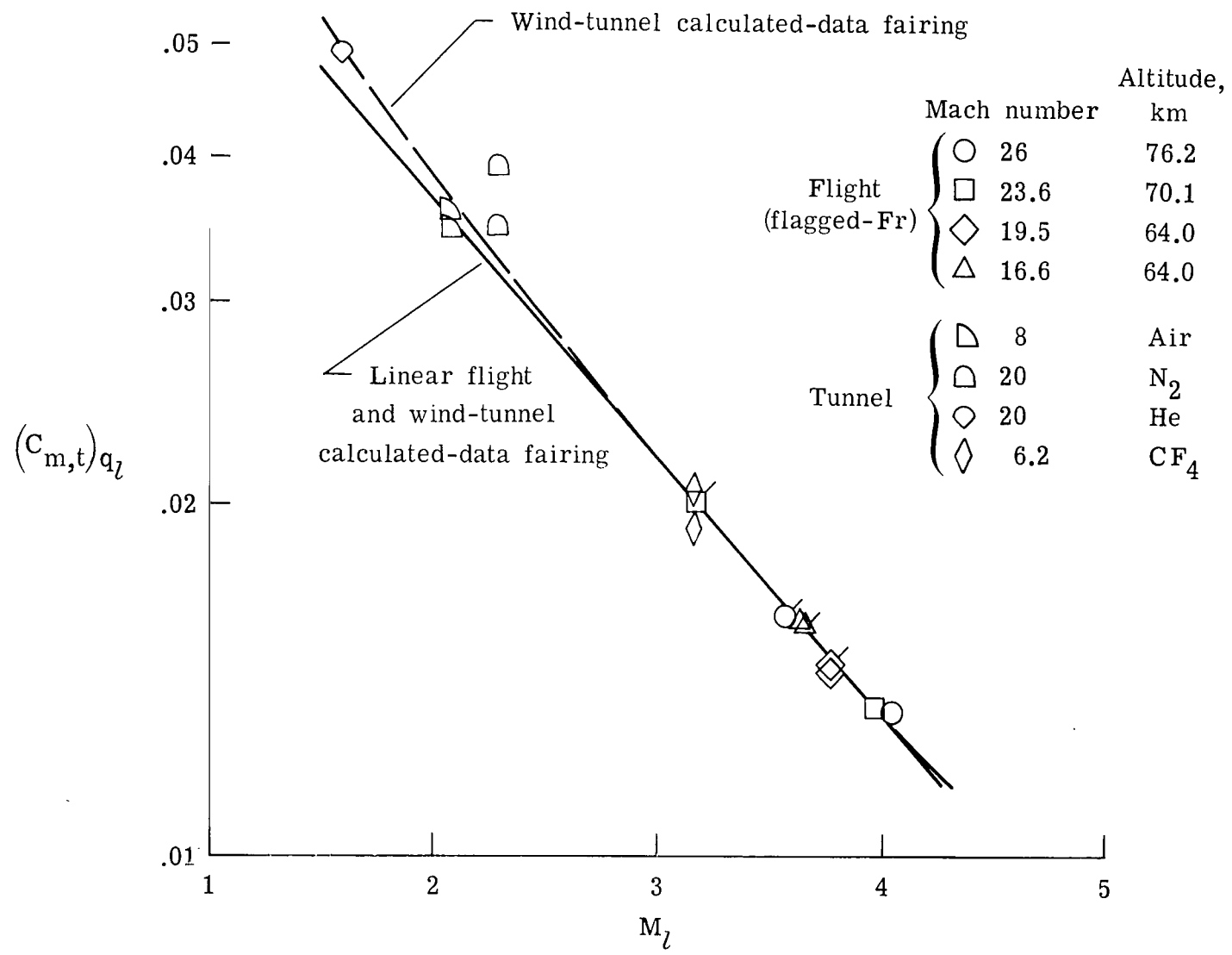
Figure 27.- Correlation of total pitching-moment coefficient (nondimensionalized by local dynamic pressure) with local Mach number.

407 CC1 C1 U   A 7706C3 S00903DS
DEET CF THE AIF FCFCE
AF WEAPONS IAECEATCRY
ATTN: TECHNICAI IIEEAEY (SUI)
KIBTIANC AFE NM 87117

*"The aeronautical and space activities of the United States shall be
conducted so as to contribute . . . to the expansion of human knowl-
edge of phenomena in the atmosphere and space. The Administration
shall provide for the widest practicable and appropriate dissemination
of information concerning its activities and the results thereof."*
—NATIONAL AERONAUTICS AND SPACE ACT OF 1958

NASA SCIENTIFIC AND TECHNICAL PUBLICATIONS

TECHNICAL REPORTS: Scientific and technical information considered important, complete, and a lasting contribution to existing knowledge.

TECHNICAL NOTES: Information less broad in scope but nevertheless of importance as a contribution to existing knowledge.

TECHNICAL MEMORANDUMS: Information receiving limited distribution because of preliminary data, security classification, or other reasons. Also includes conference proceedings with either limited or unlimited distribution.

CONTRACTOR REPORTS: Scientific and technical information generated under a NASA contract or grant and considered an important contribution to existing knowledge.

TECHNICAL TRANSLATIONS: Information published in a foreign language considered to merit NASA distribution in English.

SPECIAL PUBLICATIONS: Information derived from or of value to NASA activities. Publications include final reports of major projects, monographs, data compilations, handbooks, sourcebooks, and special bibliographies.

TECHNOLOGY UTILIZATION PUBLICATIONS: Information on technology used by NASA that may be of particular interest in commercial and other non-aerospace applications. Publications include Tech Briefs, Technology Utilization Reports and Technology Surveys.

Details on the availability of these publications may be obtained from:

SCIENTIFIC AND TECHNICAL INFORMATION OFFICE

NATIONAL AERONAUTICS AND SPACE ADMINISTRATION
Washington, D.C. 20546